

A Distributed Power Management Strategy for Multi-Paralleled Bidirectional Interlinking Converters in Hybrid AC/DC Microgrids

Pengfeng Lin^{ID}, Student Member, IEEE, Peng Wang^{ID}, Fellow, IEEE, Chi Jin^{ID}, Jianfang Xiao^{ID}, Member, IEEE, Xiaoqiang Li^{ID}, Member, IEEE, Fanghong Guo^{ID}, Member, IEEE, and Chuanlin Zhang^{ID}, Member, IEEE

Abstract—For a hybrid ac/dc microgrid (MG), bidirectional interlinking converters (BICs) enable flexible power interactions between ac and dc subgrids. In each subgrid, power sharing among diversified sources has been effectively realized by droop controllers. These power sharing concepts can also be extended to BIC applications. This paper proposes a distributed power management strategy (DPMS) for multi-paralleled BICs in the hybrid MG to avoid the overstress of a single BIC. In this strategy, each BIC is assigned with a well-devised localized distributed controller (LDC) which generates the respective power reference for the BIC. By using the LDC, BICs are allowed to exchange information with one another in the distributed communication graph. The power interactions between ac and dc subgrids can be proportionally allocated to BICs based on their different power ratings in a full distributed manner. Then the system reliability and scalability are significantly improved. Meanwhile, accurate global power sharing among all ac and dc sources in the MG would be accordingly attained. Considering the communication time delay involved in BICs, a small signal model is derived to predict the maximum tolerable delay of the studied system. The validities of the proposed DPMS and delay stability analyses are verified by a controller hardware-in-loop experimental platform.

Index Terms—Distributed power management, multi-paralleled BICs, hybrid AC/DC microgrids, global power sharing.

Manuscript received January 24, 2018; revised May 17, 2018, September 11, 2018, and November 6, 2018; accepted December 27, 2018. Date of publication January 1, 2019; date of current version August 21, 2019. This work was supported in part by the Project Renewable Energy Integration Demonstrator-Singapore in Energy Research Institute @ Nanyang Technological University and in part by the Zhejiang Provincial Natural Science Foundation of China under Grant LQ19F030008. Paper no. TSG-00125-2018. (*Corresponding author:* Peng Wang.)

P. Lin and C. Jin are with ERI@N, Nanyang Technological University, Singapore 637141 (e-mail: linp0010@e.ntu.edu.sg; jinch@ntu.edu.sg).

P. Wang is with the School of Electrical and Electronic Engineering, Nanyang Technological University, Singapore 639798 (e-mail: epwang@ntu.edu.sg).

J. Xiao is with the Faculty of Science, Agriculture and Engineering, Newcastle University, Singapore 567739 (e-mail: Jianfang.Xiao@newcastle.ac.uk).

X. Li is with the School of Electrical and Power Engineering, China University of Mining and Technology, Xuzhou 221116, China (e-mail: xqlcumt@163.com).

F. Guo is with the Department of Automation, Zhejiang University of Technology, Hangzhou 310032, China (e-mail: fhguo@zjut.edu.cn).

C. Zhang is with the College of Automation Engineering, Shanghai University of Electric Power, Shanghai 200090, China (e-mail: clzhang@shiep.edu.cn).

Color versions of one or more of the figures in this paper are available online at <http://ieeexplore.ieee.org>.

Digital Object Identifier 10.1109/TSG.2018.2890420

I. INTRODUCTION

H YBRID AC/DC microgrids (MGs) have become increasingly popular since they merge the advantages of both AC and DC MGs. AC and DC sources/loads can be coupled to the corresponding buses for reducing the power conversion stages and minimizing system costs. Around the world, several projects on hybrid AC/DC systems have been demonstrated, such as Hachinohe microgrid in Japan [1], Bronsbergen Holiday Park Netherland [2], Kythnos Greece [3] and European Supergrid [4], etc. For a given hybrid MG, the bidirectional interlinking converter (BIC) works as a critical unit bridging AC and DC buses. Nonetheless, it is worth mentioning that the rising number of distributed energy resources integrated into the MG will unavoidably result in the capacity increase of each subgrid. This would bring about larger power interactions between the two subgrids, and more power may flow through the BIC. To meet the requirements of growing subgrid capacities, instead of frequently upgrading a single BIC, a more likely way is to deploy multiple BICs connected in parallel to stack up the power exchange capacity between AC and DC subgrids. By doing so, the power flowing from the AC subgrid to the DC one or vice versa can be cooperatively shared by these BICs. Hence, the MG scalability and redundancy can be improved.

Unlike the control schemes for the single BIC in a hybrid system, power management strategies of the multi-paralleled BICs involves more challenges. In the published literature, most studies endeavor to mitigate circulating currents (CCs) among BICs since the CCs may cause extra power loss and even damage power devices. Many effective control algorithms have been proposed. For example, a common inductor is employed to form a high zero sequence impedance which significantly reduces the CCs [5]. Generation schemes of the CCs are exhaustively investigated in [6], and the CCs can be almost eliminated by adding a proportional-integral (PI) controller in the zero channel. In [7], high frequency transformers are integrated into a modular inverter system. With well-designed current controllers, the system CCs can be successfully suppressed. From the perspective of modulation, some other methods based on the space vector modulation can also be found in [8] and [9] for desirable CCs mitigations.

Apart from the CCs problem that has been commendably resolved in early studies, power sharing among interfacing converters is also an important issue in the hybrid MG. In the

DC subgrid, voltage-power (V_{dc} - P_{dc}) droop controllers ensure that the load power can be proportionally shared by distinctive sources with different power ratings [10]. In the AC network, regulated by the frequency-active power (f_{ac} - P_{ac}) droops, AC sources pick up loads and release active power in proportion to their ratings with the synchronization of f_{ac} . The same principle also applies to the reactive power (Q_{ac}) sharing by simply choosing the drooped quantity as voltage magnitude (V_{ac}) [11]. However, these control methods are parochially confined to the pure AC or DC subgrid. They cannot be directly applied to the power allocation among BICs without any modification.

To smoothly extend the power sharing concepts into the parallel BICs configuration, diverse control schemes have been analyzed. These schemes can be generally classified into centralized control and decentralized control. The former requires a central controller to communicate with all in-service BICs and broadcast power references to them. In [12], a current sharing diagram for a parallel DC-DC converter system is referred as the master-slave control. But the diagram de facto belongs the centralized control since the master controller serves as a central controller in the system. In [13], a circular chain control (3C) method is proposed for an AC MG. Yet 3C does not consider the bidirectional power flow. The control may also experience cascaded faults when an inverter is down or a commutation link fails. In [14], an advance secondary control is scrutinized for recovering the frequency and voltage in both AC and DC subgrids, whereas proportional power sharing among all sources is reserved. Taking into account of different operating modes in the MG, a hierarchical framework in [15] intends to achieve the optimal operation of the parallel converter interfaces. However, the centralized control is widely criticized to be vulnerable to single point of failures. It may not be suitable for systems that have high reliability requirements.

In contrast, the decentralized control is much preferred since the power management of BICs is independent of communication networks. In [16], droop controls are assigned to the BICs of the hybrid MG to regulate the DC subgrid bus voltage. Nonetheless, these BICs are only allowed to transfer power from the AC subgrid to the DC one, which unnecessarily deprives the BICs of bidirectional power flow functionalities. A similar drawback can be found in [17] where a DC MG is integrated into the utility grid via several BICs, and again, only unidirectional power flow is permitted. A distributed scheme in [18] is applied to adaptively modify the droop gains in a DC MG. Yet the scheme may not fit the BIC structures since it needs the information of AC current around 50Hz being propagated in communication infrastructures. This maneuver would sacrifice the signal fidelity and result in imprecise current sharing, especially when low-bandwidth communication is employed. A unified control documented in [19] asserts that it can realize proportional power allocations for BICs. However, this unified control requires the total equivalent droop gains of AC and DC subgrids, which would not be realistic since the overall droop gains may vary with the integrations of new distributed sources. Additionally, the unified method fails to obtain accurate global power sharing (GPS) among AC and DC sources due to the mismatched line impedances between

BICs and the DC bus. The autonomous operation scheme proposed in [20] introduces novel droop controls for BICs. But the accurate GPS may not be ensured since no scheme enforces the loading situations in two subgrids to be the same in steady state.

In fact, for a MG functioning for the long run, its BICs, which may be distributed far away from each other, would not be identical in terms of manufacturers, power ratings, and component parameters, etc. Yet all centralized controls discussed above overlook the discrepancies of the BIC power ratings, and simply focus on the equal power sharing among BICs. Moreover, a central controller has to be re-programmed if a new BIC needs to be installed, which compromises the system efficiencies and plug-and-play (PnP) properties. It is conceded that decentralized controls allow BICs to coordinately share the power flow. However, as in [17] and [21], droop controllers only define the power direction references only from AC to DC or from DC to AC. Bidirectional power flows are not considered and will thus not happen in real operations. Single-way power flow caused by droops stands as a barrier for the MG system expansion. The power sharing exactness can also be impaired by variant system parameters such as output impedances of the BIC DC ports.

To address above the ticklish problems, a distributed power management strategy (DPMS) is proposed in this paper for multi-paralleled BICs operation in a hybrid AC/DC MG. In the proposed strategy, all BICs are equipped with localized distributed controllers (LDCs). By using the LDCs, each BIC is allowed to exchange information with one another in more flexible communication graph. It is worth noting that the deviations of f_{ac} and V_{dc} help to determine the loading conditions of both subgrids. All BICs can detect a common f_{ac} prevailing over the AC network, but the exact V_{dc} would be imperceptible because of various line impedances between BICs and the DC bus. To balance power generations in the two subgrids and reduce communication burdens, only one BIC (defined as the leader) is allowed to receive the V_{dc} information sent by a sensor mounted on the DC bus. The remaining BICs (referred to as the followers) autonomously reach consensuses with the leader BIC such that global load balancing between AC and DC subgrids can be exactly achieved. Meanwhile, the bidirectional power flow would be precisely shared by all BICs in accordance with their different capacities, and the over-stress of a particular BIC could be avoided. Furthermore, the proposed LDCs facilitate the modularized system design. Once the controller of a newly-installed BIC is locally tuned, without reporting to a central controller, the BIC can directly join the BICs community and contribute to the power transmission. This merit is substantially favored in practical engineering with the ease of automatic PnP.

Following the introduction given by Section I, Section II shortly illustrates the droop controls in AC and DC subgrids. Section III analyzes the bidirectional power flow on BICs. A novel LDC is then proposed for multi-paralleled BICs power sharing, and an efficient design guideline for the flexible implementation of LDCs is also presented. Subsequently, a linearized small signal model is established to study the system stability with the communication time delay variations.

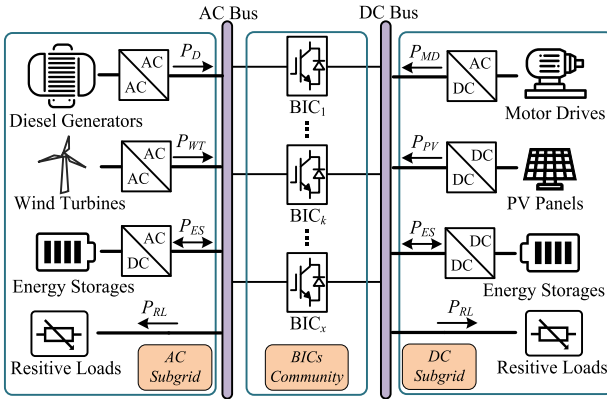


Fig. 1. Typical schematic of an autonomous hybrid AC/DC MG.

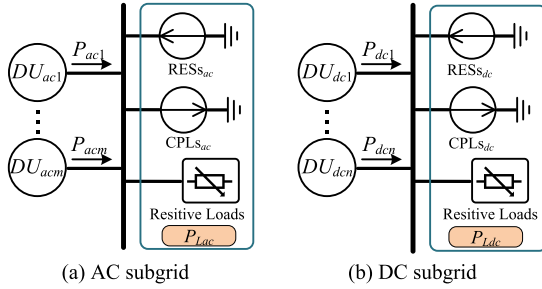


Fig. 2. Simplified schematics of the AC subgrid and the DC subgrid.

In Section IV, controller hardware-in-loop (HIL) tests verify the effectiveness of the proposed DPMS and delay stability analyses. Finally, conclusions are drawn in Section V.

II. INDIVIDUAL OPERATIONS OF AC AND DC SUBGRIDS

Fig. 1 shows a generic schematic of an autonomous hybrid AC/DC MG. Renewable energy sources (RESs), such as PV arrays and wind turbines, are operated under maximum power point tracking mode. Energy storages help to compensate the power fluctuations caused by RESs. Diesel generators work as the energy backup for both AC and DC subgrids. Resistive loads (RLs) can be directly linked to AC and DC buses without any interfacing devices. Motor drives and those power electronic loads can be modeled as constant power loads (CPLs) because of their tightly-regulated consumed power. Multiple BICs connected in parallel form a BICs community which interlinks the two subgrids. The simplified layouts of individual subgrids are demonstrated in Fig. 2. In each subgrid, the energy resources except RESs are referred as dispatchable units (DUs) and operate under droop controls. RESs, CPLs, and RLs are combined as the lumped load $P_{Ly} = P_{CPLSy} + P_{RLSy} - P_{RESSy}$, where the subscript y represents either ac or dc .

A. AC Subgrid Control

Borrowed from classical power systems, f_{ac} - P_{ac} and V_{ac} - Q_{ac} droop controllers are applied in the AC subgrid to regulate the AC bus. These droops can be expressed as follows,

$$f_{ac} = f_{ac\max} - a_{pi}P_{aci}^M, \quad i \in [1, m], \quad (1)$$

$$V_{ac} = V_{ac\max} - a_{Qi}Q_{aci}^M, \quad i \in [1, m], \quad (2)$$

where $f_{ac\max}$ and $V_{ac\max}$ are the allowable maximum AC frequency and maximum voltage amplitude. m represents the total number of AC DUs. a_{pi} and a_{Qi} are the droop coefficients,

$$\begin{aligned} a_{pi} &= (f_{ac\max} - f_{ac\min})/P_{aci\max}, \\ a_{Qi} &= (V_{ac\max} - V_{ac\min})/Q_{aci\max}. \end{aligned} \quad (3)$$

In (1) and (2), P_{aci}^M and Q_{aci}^M are the measured power processed by low pass filters (LPFs). Their dynamics are

$$\dot{P}_{aci}^M = \omega_{LPF}(P_{aci} - P_{aci}^M), \quad \dot{Q}_{aci}^M = \omega_{LPF}(Q_{aci} - Q_{aci}^M), \quad (4)$$

where ω_{LPF} is the cutoff angular frequency of LPFs. P_{aci} and Q_{aci} are the real active and reactive powers.

In an AC system with complex line impedance, the controls of active and reactive powers may not be fully decoupled. However, the virtual impedance techniques in [22] are recommended to tune the AC DU output impedances being mainly inductive, so that droop controls governed by (1), (2) are still tenable. For the implementation of virtual impedance, it is highly suggested to only counteract the resistive component of AC line impedance while remaining the inductive part being the original value. By doing so, the MG stability margin would not be markedly affected. Moreover, there is only one prevailing frequency throughout the AC network. Each AC DU proportionally contributes to the load according to its power rating. However, the error of the reactive power sharing will always exist because different terminal impedances between DUs and AC bus may cause different voltage drops. Control methods regarding the reactive power sharing improvements are documented in [23] and [24]. Yet these methods will not be discussed here since reactive power is only confined in the AC subgrid and would not exist in the DC part. Instead, this paper focuses more on the power flow coordination between AC and DC subgrids.

B. DC Subgrid Control

Due to the absence of f_{ac} and Q_{ac} , the DC subgrid has a simpler droop scheme,

$$V_{dc} = V_{dc\max} - d_j P_{dcj}^M, \quad j \in [1, n], \quad (5)$$

where $V_{dc\max}$ represents the maximum output voltage of the j th DU. d_j is the DC droop coefficient as described below,

$$d_j = (V_{dc\max} - V_{dc\min})/P_{dcj\max}, \quad (6)$$

The dynamic of ΔP_{dcj}^M is written in (7) with P_{dcj} being the real DC power,

$$\dot{P}_{dcj}^M = \omega_{LPF}(P_{dcj} - P_{dcj}^M). \quad (7)$$

Similar to the reactive power sharing in the AC subgrid, the power allocation among the DC DUs could also differ from the designated proportional distribution. This is caused by the terminal impedance disparities between DUs and DC bus. However, the intention of this paper is to realize the distributed power management of multi-paralleled BICs and GPS in the hybrid MG. The effects of terminal impedances

on system performances are assumed to be minor and can be ignored.

III. THE DISTRIBUTED POWER MANAGEMENT STRATEGY

A. Analysis of Power Flow on BICs Community

For both AC and DC networks, droop schemes give rise to the floating f_{ac} and V_{dc} which can be used to determine AC and DC loading conditions (LCs) [11]. Referring to (1) and (5), the large drop of f_{ac} (or V_{dc}) indicates that the AC (or DC) network is heavily loaded, whereas f_{ac} (or V_{dc}) would increase in the case of light load. In the hybrid MG, AC and DC subgrids coexist. They are interconnected by the BICs community which aims to coordinate the power generations between the two subgrids. Concretely, if the AC LC is detected being higher than the DC LC, then BICs will extract the power from the AC subgrid and inject it into the DC one. Conversely, the power will be channeled from the DC subgrid to the AC one when the DC LC exceeds the AC LC. By doing so, the AC and DC LCs will be equalized in steady state. All DUs in the hybrid MG proportionally supply the power to the lumped load, which means GPS has been accomplished [25].

The combined droop equations in the separated AC and DC subgrids can be written below,

$$f_{ac} = f_{ac \max} - aP_{ac}^M, P_{ac}^M = \sum_{i=1}^m P_{aci}^M, P_{ac} = \sum_{i=1}^m P_{aci}, \quad (8)$$

$$V_{dc} = V_{dc \max} - dP_{dc}^M, P_{dc}^M = \sum_{j=1}^n P_{dcj}^M, P_{dc} = \sum_{j=1}^n P_{dcj}. \quad (9)$$

It is worth mentioning that a and d in (8) and (9) are the equivalent droop coefficients which are expressed as follows,

$$a = \left(\sum_{i=1}^m a_i^{-1} \right)^{-1} = \frac{f_{ac \ max} - f_{ac \ min}}{P_{ac \ max}}, P_{ac \ max} = \sum_{i=1}^m P_{aci \ max}, \quad (10)$$

$$d = \left(\sum_{j=1}^n d_j^{-1} \right)^{-1} = \frac{V_{dc \ max} - V_{dc \ min}}{P_{dc \ max}}, P_{dc \ max} = \sum_{j=1}^n P_{dcj \ max}, \quad (11)$$

where $P_{ac \ max}$ and $P_{dc \ max}$ are the maximum active powers of the two subgrids. AC and DC LCs are defined below,

$$\text{LC}(f_{ac}) = \frac{f_{ac} - f_{ac \ max}}{f_{ac \ max} - f_{ac \ min}}, \text{LC}(V_{dc}) = \frac{V_{dc} - V_{dc \ max}}{V_{dc \ max} - V_{dc \ min}}. \quad (12)$$

Taking the scenario of $\text{LC}(V_{dc}) > \text{LC}(f_{ac})$ for example, to achieve the GPS, the difference of $\text{LC}(V_{dc})$ and $\text{LC}(f_{ac})$ will be processed to generate the active power reference (ΔP_{BICs}) for the BICs community. It should be stressed that, no matter whether the two subgrids are heavily or lightly loaded, as long as $\text{LC}(f_{ac})$ and $\text{LC}(V_{dc})$ are different, BICs would drive power flowing from the subgrid with relatively light load to another one. Once BICs are activated, the hybrid MG reaches a new operating point such that $\text{LC}(V_{dc}) = \text{LC}(f_{ac})$. At this point, droop equations given in (8) and (9) have to be refined considering the involvement of ΔP_{BICs} ,

$$f_{ac} = f_{ac \ max} - a(P_{ac}^M - \Delta P_{\text{BICs}}^M), \quad (13)$$

$$V_{dc} = V_{dc \ max} - d(P_{dc}^M + \Delta P_{\text{BICs}}^M), \quad (14)$$

where ΔP_{BICs}^M is the measured value, and the instantaneous BICs power is denoted as ΔP_{BICs} .

Applying LC calculation rules to (13) and (14) yields,

$$\text{LC}(f_{ac}) = \frac{-P_{ac}^M + \Delta P_{\text{BICs}}^M}{P_{ac \ max}}, \text{LC}(V_{dc}) = \frac{-P_{dc}^M - \Delta P_{\text{BICs}}^M}{P_{dc \ max}}. \quad (15)$$

By equating $\text{LC}(f_{ac})$ and $\text{LC}(V_{dc})$, the power flow on the BICs community can be obtained,

$$\Delta P_{\text{BICs}}^M = \frac{P_{ac}^M P_{dc \ max} - P_{dc}^M P_{ac \ max}}{P_{dc \ max} + P_{ac \ max}}. \quad (16)$$

For the scenario discussed above, the AC subgrid can be emulated as one of DC loads with an AC/DC interface (BICs community). The DC subgrid can be viewed as one of power sources in the AC subgrid. In this regard, ΔP_{BICs}^M should be contributed by all DC DUs and assigned to all AC DUs based on their respective ratings. Similar to (13) and (14), droops in (1) and (5) should be modified below,

$$f_{ac} = f_{ac \ max} - a p_i (P_{aci}^M - \Delta P_{\text{BICs}i}^M), \quad i \in [1, m], \quad (17)$$

$$V_{dc} = V_{dc \ max} - d_j (P_{dcj}^M + \Delta P_{\text{BICs}j}^M), \quad j \in [1, n], \quad (18)$$

where $\Delta P_{\text{BICs}i}^M$ is the supplementary power received by the i th AC DU. $\Delta P_{\text{BICs}j}^M$ is the additional power generated by the j th DC DU. To have an explicit view of how power allocation occurs in each subgrid, deviations of f_{ac} and V_{dc} from their maximum values before and after BIC operation can be written as follows,

Before BIC operation:

$$\begin{cases} \Delta f_{ac} = f_{ac \ max} - f_{ac} = a p_i P_{aci}^M = a P_{ac}^M \\ \Delta V_{dc} = V_{dc \ max} - V_{dc} = d_j P_{dcj}^M = d P_{dc}^M \end{cases}, \quad (19)$$

After BIC operation:

$$\begin{cases} \Delta f_{ac} = f_{ac \ max} - f_{ac} = a p_i (P_{aci}^M - \Delta P_{\text{BICs}i}^M) = a (P_{ac} - \Delta P_{\text{BICs}}^M) \\ \Delta V_{dc} = V_{dc \ max} - V_{dc} = d_j (P_{dcj}^M + \Delta P_{\text{BICs}j}^M) = d (P_{dc} + \Delta P_{\text{BICs}}^M) \end{cases}. \quad (20)$$

Manipulating (19) and (20), $\Delta P_{\text{BICs}i}^M$ and $\Delta P_{\text{BICs}j}^M$ are given as,

$$\Delta P_{\text{BICs}i}^M = \frac{a}{a p_i} \Delta P_{\text{BICs}}^M = \frac{P_{aci \ max}}{P_{ac \ max}} \Delta P_{\text{BICs}}^M, \sum_{i=1}^m \Delta P_{\text{BICs}i}^M = \Delta P_{\text{BICs}}^M, \quad (21)$$

$$\Delta P_{\text{BICs}j}^M = \frac{d}{d_j} \Delta P_{\text{BICs}}^M = \frac{P_{dcj \ max}}{P_{dc \ max}} \Delta P_{\text{BICs}}^M, \sum_{j=1}^n \Delta P_{\text{BICs}j}^M = \Delta P_{\text{BICs}}^M. \quad (22)$$

Substituting (10) and (11) into (20), and further conducting LC calculations, relations among all DUs generation across the overall MG system can be identified below,

$$\begin{aligned} \frac{P'_{aci}}{P_{aci \ max}} &= \frac{P_{aci}^M - \Delta P_{\text{BICs}i}^M}{P_{aci \ max}} = \frac{P_{ac}^M - \Delta P_{\text{BICs}}^M}{P_{ac \ max}} \\ &= \frac{P'_{dcj}}{P_{dcj \ max}} = \frac{P_{dcj}^M + \Delta P_{\text{BICs}j}^M}{P_{dcj \ max}} = \frac{P_{dc}^M + \Delta P_{\text{BICs}}^M}{P_{dc \ max}}. \end{aligned} \quad (23)$$

In steady state, the measured quantities equal the real power values. P_{aci}' and P_{dcj}' are the real active power provided by

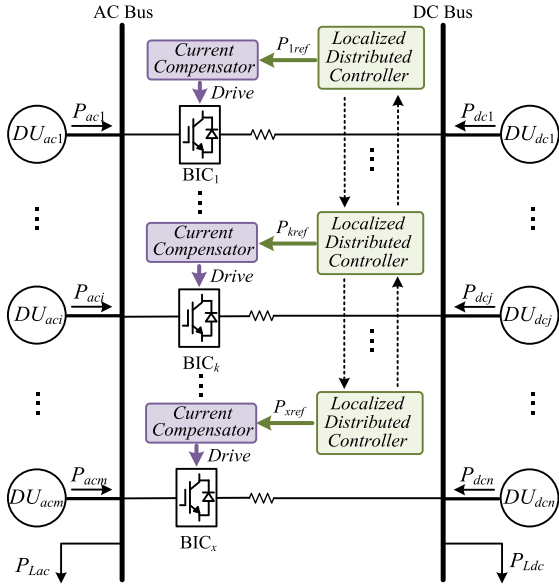


Fig. 3. Multi-paralleled BICs under the proposed DPMS.

the i th AC DU and the j th DC DU after BICs community is configured. All DUs in the hybrid MG produce the power proportional to their ratings, which means the GPS is perfectly realized.

B. The Proposed LDC

Given that the multi-paralleled BICs may have different power ratings, the concepts of power sharing in AC and DC subgrids should also be extended to the BICs community. As analyzed before, to obtain GPS, the power flow on BICs can be computed as ΔP_{BICs} . The follow-up objective is to schedule BICs to proportionally share ΔP_{BICs} . As in Fig. 3, each BIC is regulated by the proposed LDC which separately gives the respective active power reference. By using LDC, the power sharing among BICs can be realized in a fully distributed way. A particular BIC only needs to know the operation status of its nearest neighbors, which substantially improves the system PnP capability. Before proceeding to illustrate the LDC, some preliminaries pertaining to graph theory have to be introduced to better understand the related reasoning.

1) *Graph Theory*: For a network graph, there are totally N nodes $\mathcal{V} = \{v_1, v_2, \dots, v_N\}$, and $\varepsilon \subseteq \mathcal{V} \times \mathcal{V}$ represents the set of edges linking two different nodes. This graph is assumed to be undirected if $(v_k, v_l) \subseteq \varepsilon$ and $(v_l, v_k) \subseteq \varepsilon$, otherwise, it is directed [26], [27]. For MG applications, communication networks are normally modeled as undirected graph [28]. Furthermore, the set formed by the neighbors of the k th vertex can be expressed as $\mathcal{N}_k \triangleq \{v_l \subseteq \mathcal{V} : (k, l) \subseteq \varepsilon\}$. The symmetrical adjacent matrix $\mathcal{A} \subseteq \mathbb{R}^{N \times N}$ possesses components $a_{kl} = a_{lk} = 1$ if $v_l \subseteq \mathcal{N}_k$, otherwise, $a_{kl} = a_{lk} = 0$. The adjacent matrix means that node l is capable of receiving information from node k if node l is one of its neighbors, and vice versa. Laplacian matrix $\mathbf{L} \subseteq \mathbb{R}^{N \times N}$ equals $\mathcal{A} - \mathcal{D}$, where \mathcal{D} is the in-degree matrix denoted as $\mathcal{D} = \text{diag}\{d_k\} \subseteq \mathbb{R}^{N \times N}$, and $d_k = \sum a_{kl}$ if $v_l \subseteq \mathcal{N}_k$. Laplacian matrix \mathbf{L} will further be utilized in small signal stability analyses in Section III

Part D. As reported in [29], BICs can cooperatively function if the communication graph maintains at least a spanning tree. Concretely, there exists at least one BIC working as the root node such that the necessary information can be propagated to all other BICs. This BIC is defined as the leader in this paper, and other BICs are referred as the followers.

2) *LDC*: In Section III *Part A*, it has been shown that the power interaction between the two subgrids can be theoretically computed as ΔP_{BICs} which has to be transferred by the BICs community. To avoid an overstressed BIC in the MG, as in Fig. 3, the first control objective is that the sum of all BIC power references equals ΔP_{BICs} , and these references should be proportional to the respective BIC ratings,

$$\sum_{k=1}^x P_{k\text{ref}} = \Delta P_{\text{BICs}}, \frac{P_{1\text{ref}}}{P_{1\text{max}}} = \dots = \frac{P_{k\text{ref}}}{P_{k\text{max}}} = \dots = \frac{P_{x\text{ref}}}{P_{x\text{max}}}. \quad (24)$$

As emphasized earlier, GPS realizations necessitate f_{ac} of AC bus and V_{dc} of DC bus. All BICs can easily perceive f_{ac} and know the AC loading condition as there is only one dominating frequency in the AC subgrid. Unfortunately, V_{dc} cannot be locally sensed by BICs due to the existence of line impedance between BICs and DC bus. To measure V_{dc} , an excessive sensor deployed on DC bus must be used. Moreover, communication processes incurred in the BICs community should not be over complicated. High system scalabilities have to be guaranteed for the ease of modularized BIC design. In this context, apart from the constraint given in (24), the second objective is that the exact value of V_{dc} transmitted by the DC bus sensor could only be known by the leader BIC. The follower BICs are scheduled to achieve consensuses with the leader by collecting information from their neighbors. Provided that the leader BIC is down, its leading role can be randomly assigned to the rest BICs, thus ensuring normal operations of the BICs community and fortifying PnP capabilities.

In response to the two objectives formulated above, an original LDC is devised for the k th BIC, as detailed below,

$$\begin{cases} P_{k\text{ref}} = G_d(k_{kp}e_k + k_{ki} \int e_k dt) \\ e_k = \alpha_k \sum_l \left(\frac{P_{l\text{ref}}}{P_{l\text{max}}} - \frac{P_{k\text{ref}}}{P_{k\text{max}}} \right) + g_k \beta_k e_{LC} \\ e_{LC} = LC(V_{dc}) - LC(f_{ac}) \end{cases} \quad (25)$$

In (25), $\alpha_k, \beta_k \in \mathbb{R}^+$ are the proportional gains. g_k is the pinning control gain, and it is a nonzero constant for the leader BIC. e_k is the summed error processed by a proportional-integral (PI _{k}) controller. Due to the presence of PI _{k} , e_k will be forced to be zero in steady state. It is easily observed that e_k comprises two kinds of errors, $P_{l\text{ref}}/P_{l\text{max}} - P_{k\text{ref}}/P_{k\text{max}}$ and $LC(V_{dc}) - LC(f_{ac})$ respectively. For the former, $P_{l\text{ref}}/P_{l\text{max}}$ ($v_l \subseteq \mathcal{N}_k$) would be the information received from the neighbors of the k th BIC, and $P_{k\text{ref}}/P_{k\text{max}}$ denotes the localized information of the k th BIC. Upon the MG system reaching an equilibrium point, $P_{l\text{ref}}/P_{l\text{max}} - P_{k\text{ref}}/P_{k\text{max}}$ is regulated to be zero. This means the first objective given in (24) has been achieved. As for the latter, $LC(V_{dc}) - LC(f_{ac})$ only presents in the LDC of the leader BIC. This term will also converge to zero at the end of system transition, which makes sure that the GPS of the whole MG can be realized.

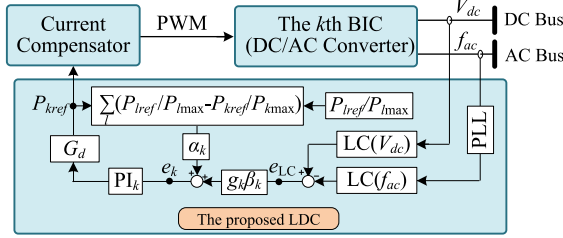
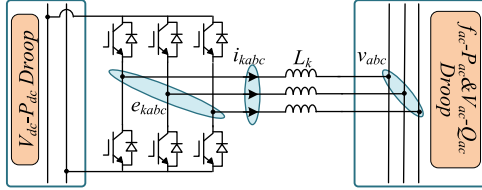


Fig. 4. Control diagram of the proposed LDC.

Fig. 5. Schematic of the k th BIC.

The control diagram of the proposed LDC is displayed in Fig. 4. It is noted that LDC involves information exchange procedures which would cause the communication time delay. For accurate modeling, the delay term G_d is included in the LDC, as justified in [15], [30],

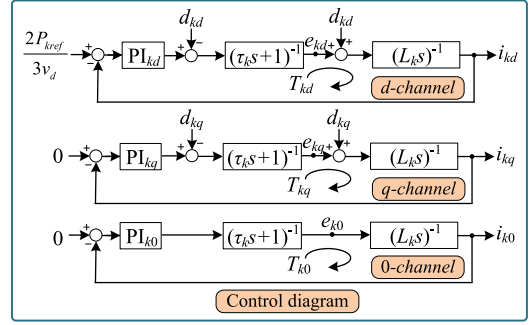
$$G_d = 1/(\tau_d s + 1), \quad (26)$$

where τ_d is the communication time delay which will be shown to possibly destabilize the MG if it is excessively large.

C. Implementation of LDC

As indicated in Fig. 3, the realization of the LDC is to send power references to current regulation loops. Corresponding gate signals will be generated and drive the switches of BICs. Besides, sampling frequencies of BICs are normally the same as switching frequencies (f_{sw}) [31]. A BIC that has larger capacity may have lower f_{sw} for the reduction of switching losses. These facts result in different control delays in different BICs. Moreover, the low f_{sw} requires the large filtering inductances to suppress high order harmonics [32]. Therefore, multiple BICs may have different f_{sw} s, control delays, and filtering inductances, etc. These dissimilarities will hinder the PnP operations, and even engender stability issues if current compensators are improperly designed. To overcome these difficulties, a flexible and efficient current compensator design guideline is developed.

For a particular BIC working as either a leader or a follower, the corresponding LDC unexceptionally gives power reference to the current compensator. The compensator further generates gate signals to drive three phase bridges so that the real power flow on the BIC could track the power reference. Fig. 5 shows the circuit schematic of the k th BIC. L_k is the filtering inductance. v_{abc} is the AC bus voltage and i_{kabc} is the inductor current. e_{abc} is the averaged output voltage of the BIC bridges. In the control diagrams (see Fig. 6), v_{abc} , i_{kabc} and e_{abc} are transformed into v_{dq0} , i_{kdq0} and e_{kdq0} respectively. τ_k denotes the control delay and usually computed as $\tau_k = 1.5T_{ksw} = 1.5/f_{ksw}$, where T_{ksw} is the switching period.

Fig. 6. Schematic of the k th BIC and its control diagram.

As proved in [31], resistors would help to stabilize the control system. To consider the worst case, equivalent resistances are not drawn in Fig. 5 and will not be embodied in the following design guideline. PI_{kd} , PI_{kq} , and PI_{k0} are current compensators which are supposed to provide sufficient response speeds and phase margins (PMs). PI_{k0} in 0 channel is to eliminate zero sequence CCs in the BICs community, as understood from [6]. $d_{kd} = -v_d + L_k 2\pi f_{ac} i_{kq}$ and $d_{kq} = -v_q - L_k 2\pi f_{ac} i_{kd}$ are disturbances in the forward path.

PI_{kd} , PI_{kq} , and PI_{k0} can be written as the following,

$$PI_{kd} = \frac{k_{kdp}s + k_{kdi}}{s}, \quad PI_{kq} = \frac{k_{kqp}s + k_{kqi}}{s}, \quad PI_{k0} = \frac{k_{k0p}s + k_{k0i}}{s}. \quad (27)$$

To begin with, as seen from Fig. 6, the open loop transfer function in d channel can be written below,

$$T_{kd} = (k_{kdp}s + k_{kdi}) / (L_k s^2 (\tau_k s + 1)). \quad (28)$$

Replacing s in (28) with $j\omega$ and doing manipulations yields,

$$T_{kd}(j\omega) = (j\omega k_{kdp} + k_{kdi}) / (j(-\omega^3 L_k \tau_k + j\omega^2 L_k)). \quad (29)$$

The control bandwidth ω_k can be determined as $2\pi f_{ksw}/\varepsilon$, where ε is a constant set as 20. At ω_k , the magnitude of $T_{kd}(j\omega)$ should be 0 dB, which can be expressed as,

$$\begin{aligned} |T_{kd}(j\omega)| &= \frac{(\omega_k k_{kdp})^2 + k_{kdi}^2}{(\omega_k^3 L_k \tau_k)^2 + (\omega_k^2 L_k)^2} = 1 \\ \Rightarrow k_{kdp} &= \frac{(\omega_k^3 L_k \tau_k)^2 + (\omega_k^2 L_k)^2}{\omega_k^2 + (k_{kdi}/k_{kdp})^2}. \end{aligned} \quad (30)$$

Additionally, the angle of $T_{kd}(j\omega)$ can be written below,

$$\begin{aligned} \angle T_{kd}(j\omega) &= \tan^{-1} \left(\frac{\omega_k^2 \tau_k k_{kdp} + k_{kdi}}{\omega_k \tau_k k_{kdi} - \omega_k k_{kdp}} \right) - 90^\circ \\ \Rightarrow \frac{\omega_k^2 \tau_k k_{kdp} + k_{kdi}}{\omega_k \tau_k k_{kdi} - \omega_k k_{kdp}} &= -\xi, \quad \xi = \tan(90^\circ - PM), \end{aligned} \quad (31)$$

where $PM \in (0, 90^\circ)$ and $\xi \in (0, 1)$. The decreased PM gives the larger ξ . To exactly compute k_{kdp} and k_{kdi} , besides (30), an auxiliary equation can be obtained by rearranging (31),

$$\frac{k_{kdi}}{k_{kdp}} = \frac{\omega_k(\xi - \omega_k \tau_k)}{1 + \xi \omega_k \tau_k}. \quad (32)$$

Combining (30) and (32), k_{kdp} and k_{kdi} are determined below,

$$k_{kdp} = \frac{L_k^2 \omega_k^2 (\tau_k \xi \omega_k + 1)^2}{\xi^2 + 1}, k_{kdi} = k_{kdp} \frac{\omega_k (\xi - \omega_k \tau_k)}{1 + \xi \omega_k \tau_k}. \quad (33)$$

With the designated k_{kdp} and k_{kdi} given in (33), the PM of the control system can be conveniently attained by theoretical calculations. As for the compensator designs in q and 0 channels, k_{kqp} , k_{kqi} , k_{k0p} and k_{k0i} can also be easily identified by referring to the process from (30) to (33).

D. Communication Time Delay Stability Analysis

In the previous contexts, a LDC, which serves as a power regulator for the accompanied BIC, is allowed to receive/transmit data from/to its neighbors. This information exchange process inevitably introduces the communication time delay which would slow down the system response and even cause power oscillations. Therefore, it is essential to scrutinize the impacts of the time delay on the overall MG performances. To model the system, two considerations have to be made. Firstly, for a particular BIC shown in Fig. 3, the complete control includes a LDC as the outer loop and a current compensator as the inner loop. The inner loop has much higher control bandwidth and can be viewed as a unity gain when only dynamics of the outer loop are studied, as endorsed by [33]. Secondly, MG behaviors are mainly dominated by the interaction between the AC and DC droops, and BICs power flow. For simplicity, in each subgrid, multiple droops are combined into the equivalent ones as in (8) and (9). Only the merged droops as well as LDC dynamics are considered in the subsequent stability analysis since they are the main factors that may impair the MG stability, as understood from [34].

Taking into account of LPFs, rewriting (13) and (14) yields,

$$\begin{cases} \dot{f}_{ac} = -\omega_{LPF} f_{ac} + \omega_{LPF} f_{ac \max} - a\omega_{LPF}(P_{ac} - \Delta P_{BICs}) \\ \dot{V}_{dc} = -\omega_{LPF} V_{dc} + \omega_{LPF} V_{dc \max} - d\omega_{LPF}(P_{dc} + \Delta P_{BICs}) \end{cases}, \quad (34)$$

where ΔP_{BICs} is the summed power flow on BICs.

The compact form of the first equation in (25) are,

$$\tau_d \dot{\mathbf{P}}_{ref} = -\mathbf{P}_{ref} + \mathbf{k}_p \mathbf{e} + \mathbf{k}_i \boldsymbol{\phi}, \dot{\boldsymbol{\phi}} = \mathbf{e}, \quad (35)$$

where $\mathbf{P}_{ref} = [P_{1ref} \cdots P_{kref} \cdots P_{xref}]^T$, $\mathbf{k}_p = diag(k_{1p} \cdots k_{kp} \cdots k_{xp})$, $\mathbf{k}_i = diag(k_{1i} \cdots k_{ki} \cdots k_{xi})$, $\tau_d = I_{x \times x} \tau_d$ and $I_{x \times x}$ is an identity matrix with x dimensions. $\boldsymbol{\phi}$ is a state vector induced by integrators in (25). \mathbf{e} is an error vector with components e_k , which is given in (36),

$$\mathbf{e} = \alpha \mathbf{L} \mathbf{P}_{max}^{-1} \mathbf{P}_{ref} + \mathbf{G} \boldsymbol{\beta} \mathbf{1}_x \left[\frac{V_{dc} - V_{dc \max}}{\Delta v} - \frac{f_{ac} - f_{ac \max}}{\Delta f} \right], \quad (36)$$

where $\boldsymbol{\beta} = diag(\beta_1 \cdots \beta_k \cdots \beta_x)$, $\mathbf{P}_{max} = diag(P_{1max} \cdots P_{kmax} \cdots P_{xmax})$, $\mathbf{G} = diag(g_1 \cdots g_k \cdots g_x)$, $\alpha = diag(\alpha_1 \cdots \alpha_k \cdots \alpha_x)$. $\mathbf{1}_x$ is a column vector with all elements being 1.

Combining (34), (35) and (36), and performing small signal disturbance, the linearized form of the MG system is below,

$$\begin{bmatrix} \dot{\tilde{f}}_{ac} \\ \dot{\tilde{V}}_{dc} \\ \dot{\tilde{\mathbf{P}}}_{ref} \\ \dot{\tilde{\boldsymbol{\phi}}} \end{bmatrix} = \begin{bmatrix} -\omega_{LPF} & 0 & a\omega_{LPF} \mathbf{1}_x^T & 0 \\ 0 & -\omega_{LPF} & -d\omega_{LPF} \mathbf{1}_x^T & 0 \\ -A_f & A_v & B & \tau_d^{-1} \mathbf{k}_i \\ -G \boldsymbol{\beta} \mathbf{1}_x / \Delta f & G \boldsymbol{\beta} \mathbf{1}_x / \Delta v & -\alpha \mathbf{L} \mathbf{P}_{max}^{-1} & 0 \end{bmatrix} \begin{bmatrix} \tilde{f}_{ac} \\ \tilde{V}_{dc} \\ \tilde{\mathbf{P}}_{ref} \\ \tilde{\boldsymbol{\phi}} \end{bmatrix}, \quad (37)$$

where $A_f = \tau_d^{-1} k_p G \boldsymbol{\beta} \mathbf{1}_x / \Delta f$, $A_v = \tau_d^{-1} k_p G \boldsymbol{\beta} \mathbf{1}_x / \Delta v$, $B = \tau_d^{-1} (k_p \alpha \mathbf{L} \mathbf{P}_{max}^{-1} - I_{x \times x})$, $\Delta f = f_{ac \max} - f_{ac \min}$ and $\Delta v = V_{dc \max} - V_{dc \min}$.

It should be mentioned that (37) delineates the dynamics of a generalized model consisting of x BICs. For quantitative interpretations, a specific system that includes an AC DU, a DC DU, and three BICs is considered, as shown in Fig. 7. These DUs are regulated under the consolidated AC and DC droops written in (8) and (9). By doing so, the AC (or DC) subgrid can be emulated by only one AC (or DC) DU. It is further assumed that both subgrids have comparable capacities which are 40 kW. This means that loads in the hybrid MG should be evenly shared by the two DUs in steady state. The power rating ratio of three BICs in Fig. 7 is designed as $P_{1 \max} : P_{2 \max} : P_{3 \max} = 3:2:1$. The reference directions of power flow have been clearly defined. Referring to Section III Part B, in this MG, BIC₁ is configured as the leader and the others are the followers. All BICs have the similar LDC structures, which allows setting PI controllers in (25) to be identical, i.e., $\mathbf{k}_p = k_p I_{3 \times 3}$ and $\mathbf{k}_i = k_i I_{3 \times 3}$. The Laplacian matrix depicting the communication graph in Fig. 7 is $\mathbf{L} = [1 \ -1 \ 0; \ -1 \ 2 \ -1; \ 0 \ -1 \ 1;]$.

Key system parameters and the corresponding descriptions have been summarized in TABLE I. Fig. 8 shows the eigenvalue loci of the dynamic system of (37) with communication time delay τ_d varying from 0.1s to 1.2s with the step of 0.1s. Eigenvalues that have real parts less than -3.5 are not plotted in Fig. 8 as they would not aggravate the system stability and only dominant poles are presented. It is apparent that conjugate eigenvalues $-1.7 \pm j57.3$ have the negative real part when $\tau_d = 0.5s$, which means the MG is stable. The transient oscillation frequency is estimated as 9.2Hz. The oscillation frequency is approximated as 6.3Hz ($-0.3 \pm j40$) with τ_d being set as 0.8s. Unfortunately, in the case that τ_d is enlarged to be 1s, dominant poles pass through the imaginary axis and enter into the right half plane. The corresponding oscillation frequency of the unstable system is around 6Hz. Besides, as observed from Fig. 8, the studied hybrid MG can withstand communication time delay no more than 0.9 s, otherwise, the system will be destabilized. All these findings will be substantiated by experiments in the next section.

E. Discussions

1) *DC Bus Voltage Selection:* As expounded in [35], the selection of DC voltage for MGs currently lacks standardizations. Different voltage levels would accommodate distinguished applications, ranging from household appliances to common facility devices. Concretely, voltage levels of 24~48V are mainly used for electronic equipment with low

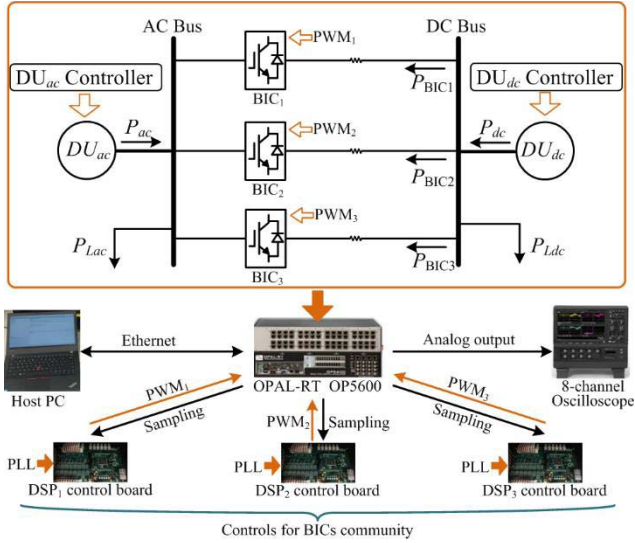


Fig. 7. The full schematic diagram of HIL tests.

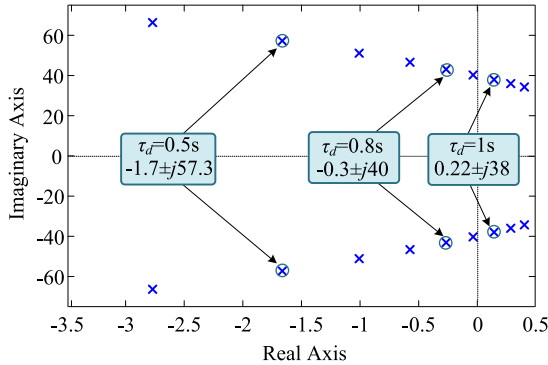


Fig. 8. Eigenvalue loci with communication time delay variations.

power ratings, including Wi-Fi routers, phone chargers, computers and LED lights, etc. For the medium power elements comprising stove ovens, dishwashers and washing machines, voltage levels of 230~240V are commonly employed. To further improve power rating and energy conversion efficiencies, 380~750V voltages could be utilized. These voltage levels are specifically suitable for common infrastructures, such as data centers (380V), electrical vehicles (400V) and tram power systems (750V), etc. For the hybrid AC/DC MG studied in our manuscript, nominal AC voltage level is selected as the standard residential voltage in China, i.e., RMS220V/50Hz. AC voltage amplitude can be identified as $220V * 1.414 = 311V$. To bridge AC and DC buses as well as guarantee the proper modulation of BICs, the nominal DC bus voltage should be more than $311V * 2 = 622V$, and in this paper, the DC voltage level is chosen as 700V. Further stipulating that the maximum voltage deviation from the nominal level is 10V, hence, as shown in Table I, the maximum DC bus voltage ($V_{dc\max}$) and the minimum DC bus voltage ($V_{dc\min}$) could be figured out as 710V and 690V respectively.

2) *Line Impedance Impacts:* In fact, the DPMS mechanism can be implemented no matter whether there are line impedances between BICs community and subgrid buses.

TABLE I
SYSTEM PARAMETERS

Parameter	Description	Value
$f_{ac\max}$	Maximum AC frequency	51Hz
$V_{dc\max}$	Maximum DC bus voltage	710V
$f_{ac\min}$	Minimum AC frequency	49Hz
$V_{dc\min}$	Minimum DC bus voltage	690V
$P_{ac\max}, P_{dc\max}$	AC power rating, DC power rating	40kW
$P_{1\max}$	Power rating of BIC ₁	6kW
$P_{2\max}$	Power rating of BIC ₂	4kW
$P_{3\max}$	Power rating of BIC ₃	2kW
ω_{LPF}	Cutoff angular frequency of LPF	500
k_p	Proportional gain in LDC	2
k_i	Integral gain in LDC	800
a_1, a_2, a_3, β_1	Proportional gains in LDC	2
g_1, g_2, g_3	Pining control gains in LDC	1, 0, 0
L_1, L_2, L_3	BIC Inductances	8e-3H
$f_{1sw}, f_{2sw}, f_{3sw}$	Switching frequencies of BICs	10kHz, 15kHz, 20kHz

Observing the mathematical expression of LDC in (25), for BIC_k, the power reference is generated by a PI controller who processes two types of errors, $P_{lref}/P_{lmax} - P_{kref}/P_{kmax}$ and $LC(V_{dc}) - LC(f_{ac})$ respectively. These errors will be enforced to be 0 in steady state, which means that the global power balancing and proper power allocation among BICs have been achieved. In LDC, no line impedance information is involved. This fact implies that impedance variations would not affect the correct functioning of the proposed control strategy at all. Furthermore, as documented in [36], the increases of line inductances tend to narrow down the system stability margin. In contrast, the stability could be enhanced by appositely increasing line resistances since resistive components could contribute damping effects to the MG. Therefore, despite that AC and DC subgrids are interlinked via BICs in a single points or multiple points, it is recommended to incorporate small line resistors to ensure stable operations. During HIL tests in this paper, small resistors are added between BICs and DC bus for improving system stability. On the other hand, it is admitted that the line resistance in the DC subgrid may affect the accurate power sharing among DC DUs. Distributed control scheme similar to (25) can be devised to generate the correcting items that are imposed to DC droop controllers. Then the proportional power allocation in DC DUs could be rigorously achieved. Upon this situation, the negative value of normalized power quantity in any DC DU could be used as the DC loading condition index. The index further helps to identify the BIC power flow, thus realizing the global power balancing in the hybrid MG.

3) *Dynamic Decoupling of Droops and LDCs From DU Voltage Controllers:* The power circuit and control diagram of a given DU_{ac} can be found in Fig. A1. Droop controllers with LPFs generate voltage reference for the voltage control loop to properly regulate AC bus. It is worth noting that the control bandwidth of the voltage control is normally designed being much higher than LPF-enabled droop controllers and LDCs.

LDCs and the voltage loop are functioning in different time scales. Since AC bus capacitor dynamics have been fully incorporated in the voltage control, the proposed LDCs are hence almost in no relation to AC bus capacitance. Similar results can also be obtained from Fig. A2 where DC droop has far slower dynamic than the voltage tracking loop. Voltage control loops in DU_{ac} and DU_{dc} can be viewed as unity gains when droop characteristics are investigated. For these reasons, as suggested by [37], only droop controllers are necessarily taken into account of stability analyses and those voltage controls could be neglected.

4) Phase Locked Loop (PLL) Impacts: In BIC controls, AC frequency could be sensed by traditional PLL (see Fig. A4). As detailed in [38], PLL formulates a transfer function from the real frequency to the frequency utilized in BIC controls. This transfer function is essentially a second-order LPF which would slow down frequency measuring dynamics and fail to incur any stability issues to the overall hybrid MG. Besides, PLL refrains from affecting d channel current controller in BICs, but imposes excessive terms to q channel. Although the imposed terms may destabilize the BIC system by interacting with AC subgrid impedance, the destabilizing effects could be completely eliminated through introducing terminal voltage feedforward control [38]. In this regard, it is fair to reach that PLL exerts little impacts to the proposed power management strategy in this paper.

5) System Performances Under Communication Loss: Centralized controls may suffer from single point of failures, which means that the whole system would collapse when a critical device is damaged. In contrast, the proposed distributed scheme helps to enhance the resilience against communication losses. In Fig. 4, if BIC_k is isolated from the communication network and operates in an autonomous way, the integrator of PI controller in LDC records the power reference that is generated right before communication failure. The reference value maintains unchanged until the failure is cleared, and BIC_k continues to transfer power from one subgrid to another. As for the rest BICs, as long as their communication graph is in spanning tree form, the global power balancing of two subgrids and the power sharing among these BICs can still be achieved without being affected at all.

IV. HARDWARE-IN-LOOP (HIL) VERIFICATION

To validate the proposed DPMS for multi-paralleled BICs, an in-house controller HIL experimental platform is established as in Fig. 9. The corresponding schematic has been plotted in Fig. 7. The switching models of DUs and their associated controls are firstly developed in OP5600 simulator to form up the two subgrids with droop features. Each DU model is allocated to a CPU core in OPAL-RT platform for the escalation of computation speed. BIC power circuits are also modeled in the real-time simulator, whereas the current compensators and LDCs are realized in Digital Signal Processor (DSP) controller boards. The inputs of DSPs are voltage and current measurements, which are converted from digital signals in the simulation model to the analog signals by the D2A terminals of OPAL-RT system. PLL algorithm

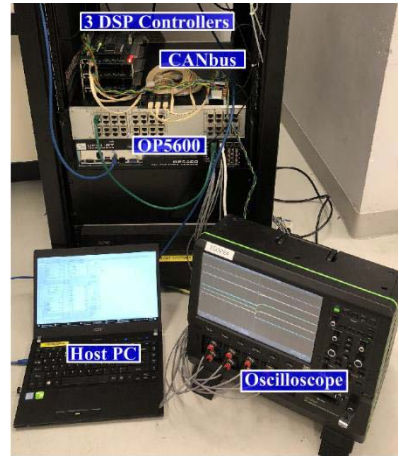


Fig. 9. Physical setup of HIL tests.

is realized in each DSP to extract the frequency information and phase angle for unity power factor operations. The outputs of the DSP controller boards are PWM signals, which will be sent to the PWM channels of OPAL-RT system and then drive the power switches in the BIC models.

DSPs communicate with one other by CANbus which supports baud rate up to 1Mbps. Conceding that RS232 series communication protocol is quite popular in power engineering applications, yet its data transition rate is normally 115200bps, which is comparatively slow [23]. Although Modbus TCP/IP allows for higher speed and longer distance, establishing such a complete communication network is relatively costly [2]. Making a trade-off between efficiency and capital cost, the CANbus protocol is thus selected and implemented in HIL tests. Then the effectiveness and feasibility of DPMS are corroborated by the following four cases. Case 1 tests the PnP functionalities of BICs. Case 2 considers an aberrant situation that the leading role of BIC_1 is transferred to BIC_2 due to the BIC_1 outage. Case 3 scrutinizes the bidirectional power flow of the BICs community. Differing from the above cases, case 4 studies the impacts of the increased τ_d on overall system stability, which vindicates the observations in the last section.

A. Case 1: PnP Function Tests

Fig. 10 demonstrates the scenario that three BICs in Fig. 7 are enabled in sequence. As plotted in Fig. 10 (a), before BICs operation, AC and DC subgrids are feeding loads of around 12.84kW and 0.92kW respectively. Since the two subgrids have equal capacities, it is easily reasoned that the AC subgrid is heavily loaded and DC loads are light. To globally balance the loads in the entire hybrid MG, the BICs community should be dispatched to channel the power from the DC subgrid to the AC one. Once the BIC_1 is enabled, the output power of the two subgrids could converge to the same value which is 6.86kW, and BIC_1 power is read as 5.95kW. Next, when BIC_2 is triggered to avoid the overstress of BIC_1 , BIC_2 power immediately increases to 2.38kW while BIC_1 power quickly drops to 3.57kW, as shown in Fig. 10 (b). It should be emphasized that the summed power flow of the two BICs equals 5.95 kW which is previously transferred by only BIC_1 .

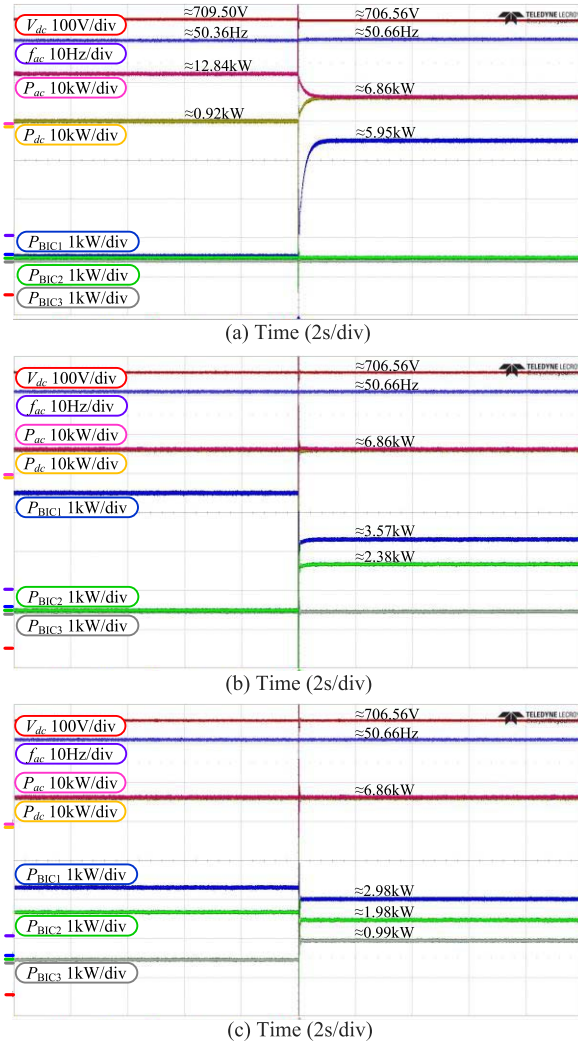


Fig. 10. Experimental results of case 1: (a) BIC₁ is enabled; (b) BIC₂ is enabled; (c) BIC₃ is enabled.

The power interaction between AC and DC subgrids keeps unchanged even in the case of BIC₂ is involved. Moreover, f_{ac} and V_{dc} are also unaffected, and they are stabilized at 50.66Hz and 706.56V respectively. Similar results can also be found when BIC₃ is activated. As evident in Fig. 10 (c), the total power flow on the BICs community is proportionally allocated to the three BICs whose power can be estimated as 2.98kW, 1.98kW, and 0.99kW. The ratio of these three quantities is approximately 3:2:1, which is in good agreement with the expectation in Section III Part D. GPS in hybrid MG has also been precisely realized.

Summarily, the proportional power sharing among BICs with different power ratings can be perfectly achieved by using the proposed distributed power management method. This method also reinforces PnP functionalities of the MG and facilitates the modularized system design, which is highly preferred in engineering practitioners.

B. Case 2: Leading Role Transition

Upon the equilibrium point described in Fig. 10 (c), case 2 further takes into account that both power circuit and the

controller board of BIC₁ (leader) are faulty. All PWM signals are disabled, the relays installed on AC and DC sides of BIC₁ should be turned off. Note that BIC₂ and BIC₃ are still communicating with each other, and their communication network remains as a spanning tree. This means, as long as either BIC₂ or BIC₃ is scheduled as a leader, the global power balancing of the two subgrids and the power sharing of BIC₂ and BIC₃ can still be obtained. As an exemplification, leading role transition from BIC₁ to BIC₂ is demonstrated. At the instant that BIC₁ is down, its power sharply decreases to zero. Fortunately, the power of BIC₂ and BIC₃ would instantaneously rise to 3.97kW and 1.98kW. The power ratio is approximated as 2:1, which again shows that the proper power sharing of BICs can be effectively accomplished. The powers supplied DU_{ac} and DU_{dc} maintain invariant at 6.8kW, which suggests that GPS keeps unaffected by the BIC₁ outage. As revealed by this case, the system fault tolerant capability can also be strengthened under the proposed distributed control strategy.

C. Case 3: Bidirectional Power Flow on BICs

Above two cases have explored the global power balancing such that the DC subgrid supplies the power to the AC subgrid. Without loss of generality, case 3 will perform the bidirectional power flow tests for the BICs community. Following the steady state point in Fig. 10 (c) wherein three BICs are under normal operations, in Fig. 12, DC loads and AC loads are increased sequentially. Specifically, as reported in Fig. 12 (a), power flow inversion of BICs unsurprisingly happens when load power in the DC subgrid rises. This suggests that the AC subgrid has relatively lighter loads in comparison with its DC counterpart, and the AC network would deliver power to the DC one. As identified from Fig. 12 (a), after the DC load step-up is exerted, the power flows on BICs are -3.04kW, -2.03kW, -1.01kW, which adheres to the power sharing rules as stipulated in Section III Part B. The total loads distributed in the hybrid MG are equally shared by AC and DC subgrids, and their output power can be measured as 18.85kW. Accordingly, f_{ac} and V_{dc} decline to 50.06Hz and 700.6V respectively.

When it comes to the AC load step-up (see Fig. 12 (b)), the AC subgrid sustains the atrocious loading situation. f_{ac} reduces to around 49.46Hz, almost reaching the allowable minimum AC frequency. V_{dc} can be read as 694.60V. To mitigate the overstress of the AC network, the DC subgrid helps to share the AC loads, and the output power of the two subgrids is nearly 30.79kW. BICs power flows return to be positive values which are recognized as 2.60kW, 1.74kW, and 0.87kW. The power ratio can be computed as 3:2:1, which matches the anticipation in Section III Part B.

D. Case 4: Effects of the Prolonged τ_d on System Stability

As stressed earlier, distributed control strategy unavoidably causes communication delay in the BICs community. The delay τ_d acts as a critical parameter that may narrow down the overall stability margin. In this regard, case 4 concentrates on dynamic system performances under different delay settings. Returning to the operation in Fig. 10 (a) where only BIC₁ is operated and the other BICs are in stand-by mode, when

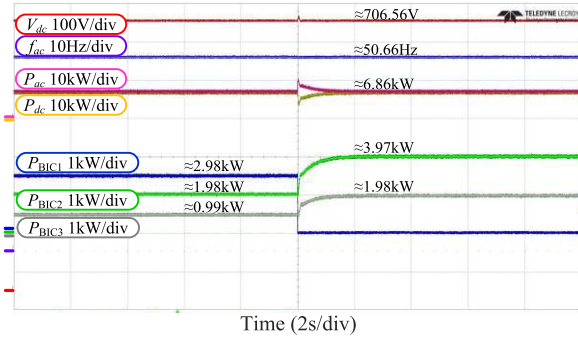


Fig. 11. Experimental results of case 2.

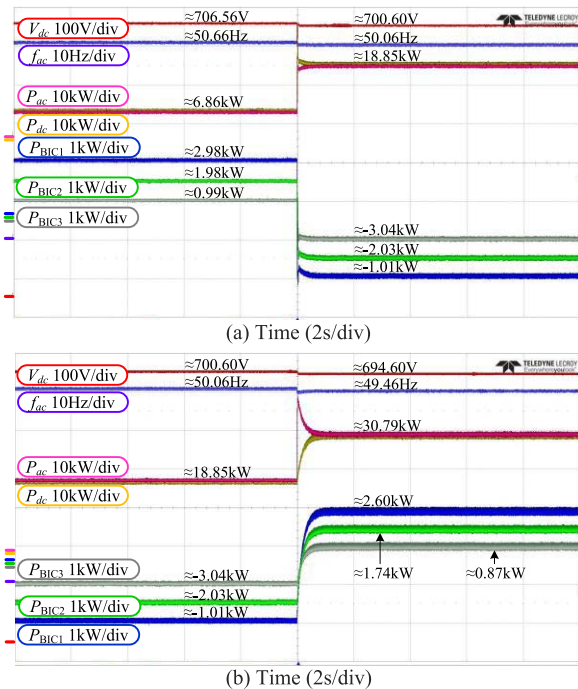
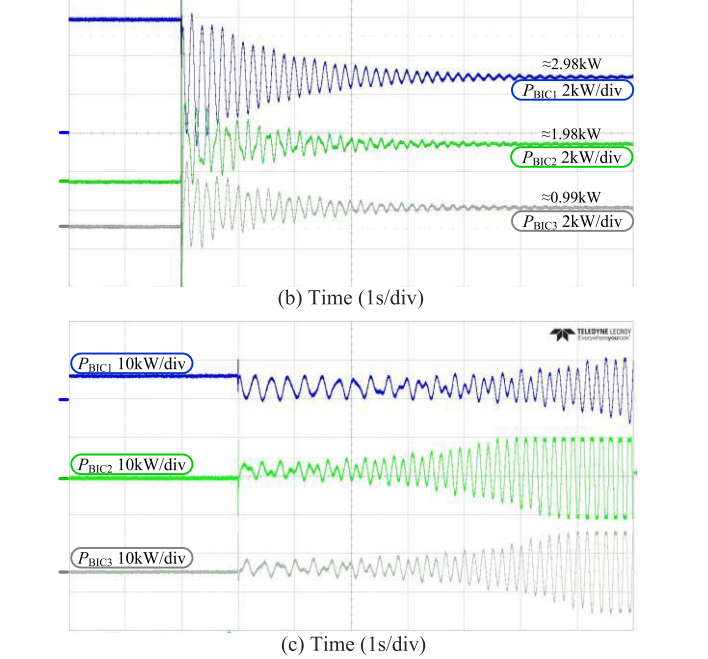
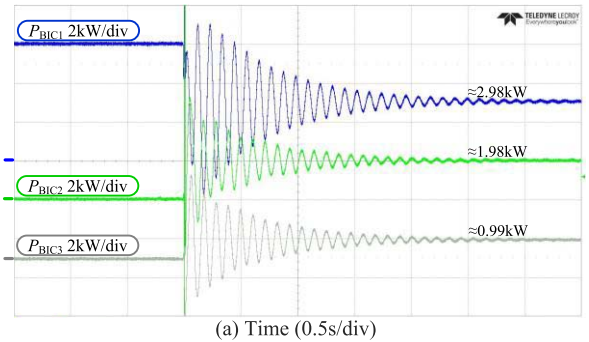


Fig. 12. Experimental results of case 3. (a) Power flow from the AC subgrid to the DC subgrid. (b) Power flow from the DC subgrid to the AC subgrid.

BIC₂ and BIC₃ are enabled concurrently, transient BIC power oscillations are recorded in Fig. 13. In the case of $\tau_d = 0.5$ s, as in Fig. 13 (a), the BICs community is under-damped and the power oscillation frequency is inspected as round 9.2Hz. This observation is consistent with eigenvalue behavior analyses presented in Section III Part D. When τ_d is deliberately escalated to 0.8s, the oscillation frequency is around 6.2Hz which is close to the expected value 6.3Hz. A worse scenario is that τ_d is boldly prolonged to 1s, which exceeds the allowable time delay (0.9s) indicated by Fig. 8. The BICs community is unstable and the power oscillates at about 6Hz. This consequence is in line with previous theoretical derivations. Therefore, to ensure the stable operation of the studied hybrid MG, the system communication delay should be strictly limited within 0.9s. With regard to the damped power oscillations in Fig. 13 (a)(b), the oscillating frequencies (9.2Hz and 6.2Hz) are arguably far less than the DC voltage regulation dynamics. From the perspective of DC bus, BIC powers are almost

Fig. 13. Experimental results of case 4. (a) $\tau_d = 0.5$ s. (b) $\tau_d = 0.8$ s. (c) $\tau_d = 1$ s.

invariant and BICs could be regarded CPLs or CPSs. As long as DC bus is properly controlled by the DU_{dc} to accommodate the wide CPL operations, the oscillated BIC powers as in Fig. 13 (a)(b) will not cause any CPL-related instability issues to the DC network.

V. CONCLUSION

In this paper, the proposed DPMS smoothly extends the power sharing concepts to the multi-paralleled BICs configuration in the hybrid AC/DC MG. Each BIC is accompanied by a novel LDC which produces the respective power reference. By means of the LDC, bidirectional power flows between AC and DC subgrids would be precisely distributed into BICs in accordance with their various power rating. In this way, an overstressed BIC can be avoided, and GPS across the entire hybrid MG can also be accomplished. A flexible and efficient current compensator design guideline is presented for the enhancements of the system modularization. Then the impacts of communication time delay on overall MG system stability are carefully studied by using a linearized small signal

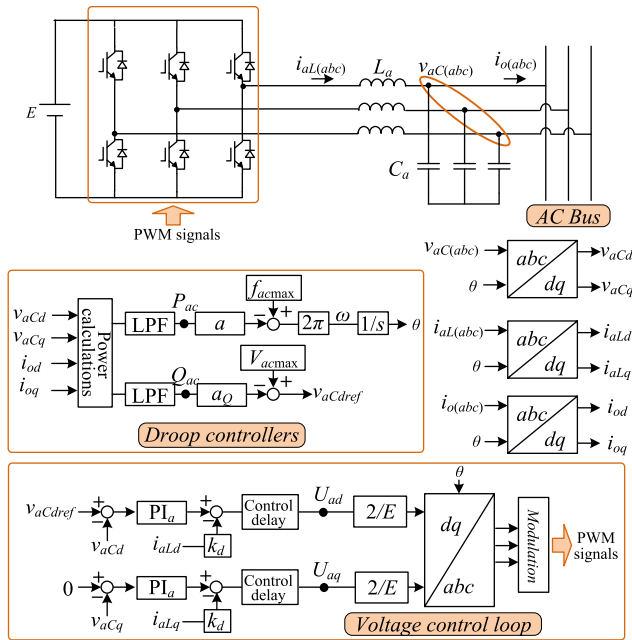
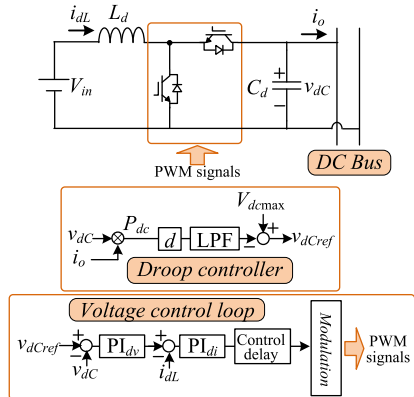
Fig. A1. Inverter based DU_{ac} circuit and control diagram.

Fig. A2. Boost converter based DUDc circuit and control diagram.

model. In-house HIL experiments validate the effectiveness of the proposed distributed control strategy.

APPENDIX

A. Control Diagrams of DU_{ac} and DU_{dc}

Fig. A1 and Fig. A2 illustrate the power circuits and the control diagrams of an inverter based DU_{ac} and a boost converter based DU_{dc} respectively. Corresponding descriptions and values have been detailed in TABLE II and TABLE III. For DU_{ac}, the voltage on AC capacitor is regulated in dq rotating frame. Conventional PI controller is adopted, and inductor current is fed back to the controller with k_d for damping the potential resonance of the LC filter. Regarding DU_{dc}, famous double loop PI controllers are used to regulate the DC bus voltage subjected to droop equation. It is worth noting that the voltage control loops in DU_{ac} and DU_{dc} are normally designed to bear high control bandwidths so that they could respond to droop controllers stably and rapidly. In this sense, it is safe to conclude

TABLE II
PARAMETERS FOR FIG. A1

Parameter	Description	Value
L_a	AC inductor	1.5mH
C_a	AC bus capacitor	60uF
a	Active power droop gain	2/40000
a_Q	Reactive power droop gain	2e-4
k_{ap}	Proportional gain in PI _a	8.2
k_{ai}	Integral gain in PI _a	246
k_d	Damping factor	20.25
E	Input DC voltage	700V
f_{sw}	Switching frequency	20kHz

TABLE III
PARAMETERS FOR FIG. A2

Parameter	Description	Value
L_d	DC inductor	2mH
C_d	DC bus capacitor	470uF
d	DC droop gain	20/40000
k_{dvp}	Proportional gain in PI _{dv}	5.35
k_{dvi}	Integral gain in PI _{dv}	2800
k_{dip}	Proportional gain in PI _{di}	0.089
k_{dii}	Integral gain in PI _{di}	280.5
V_{in}	Input DC voltage	380V
f_{sw}	Switching frequency	20kHz

that droop controllers dominate the holistic DU performances. When analyzing system stability, only droops should be necessarily considered, whereas voltage control loops could be rationally neglected.

B. Inertia Emulation by LPF

In this paper, not only do LPFs inbuilt in droop controllers help to filter the measured powers, they also contribute emulated inertia to both AC and DC subgrids for smoothing f_{ac} and V_{dc} variations. The control diagram of a synchronous generator for frequency regulation and its droop characteristic are plotted in Fig. A3 [39]. G_s represents the transfer function of speed governor and turbine. G_s could be simplified as a unity gain given that only system inertia is of interest. $P_{M,pu}$ and $P_{G,pu}$ are the mechanical power produced by prime mover and the electrical power injected into electrical grid, both denoted in per-unit (pu). The base value for power is P_{rated} , and the base value for frequency is f_{rated} .

From Fig. A3, the relationship between the instantaneous P_G and f_{ac} can be written below,

$$f_{ac,pu} = f_{ac \max,pu} - \frac{R_d}{JR_d s + R_d D + G_s} P_{G,pu} \\ \Rightarrow f_{ac} = f_{ac \max} - \frac{f_{rated}}{P_{rated}} \frac{R_d}{JR_d s + R_d D + 1} P_G, \quad (A1)$$

where J is inertial constant. Assuming that few power losses occur in the generator, and hence, damping constant D approximates to 0. (A1) can be modified as

$$f_{ac} = f_{ac \max} - \left(\frac{f_{rated} R_d}{P_{rated}} \right) \left(\frac{1/JR_d}{s + 1/JR_d} \right) P_G. \quad (A2)$$

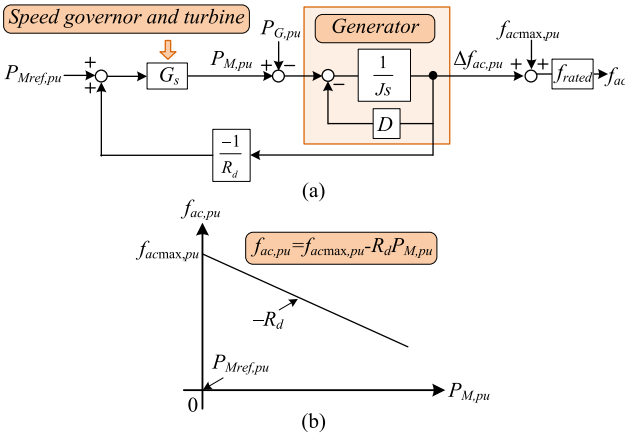


Fig. A3. (a) Control diagram of frequency regulation of a synchronous generator. (b) Droop control for the generator.

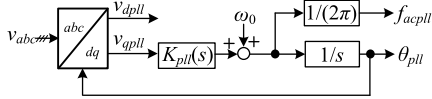


Fig. A4. Block diagram representation of PLL.

where \$(f_{rated}R_d)/P_{rated}\$ is the equivalent droop gain revealed by the synchronous generator. The mechanical inertia \$J\$ is concretized in a LPF smoothing the frequency responses. For the droop control utilized in this paper, in AC subgrid, (8) can be rewritten as

$$f_{ac} = f_{acmax} - a \frac{\omega_{LPF}}{s + \omega_{LPF}} P_{ac}. \quad (\text{A3})$$

Matching the coefficients in (A2) and (A3) gives

$$a = \frac{f_{rated}R_d}{P_{rated}}, \omega_{LPF} = \frac{1}{JR_d} \Rightarrow J = \frac{f_{rated}a}{\omega_{LPF}P_{rated}}. \quad (\text{A4})$$

The equivalent inertia devoted by LPF based droop controller is \$(f_{rated}a)/(\omega_{LPF}P_{rated})\$. The lower \$\omega_{LPF}\$ results in larger emulated inertia which would reduce the changing rate of \$f_{ac}\$. This fact allows engineers to obtain the designated frequency responses for ensuring safe operations of rotating devices like induction motors, etc. For the DC droop delineated by (9), resembling (A4) and replacing \$f_{rated}\$ with \$V_{rated}\$, the equivalent inertia can be written as

$$J = \frac{V_{rated}d}{\omega_{LPF}P_{rated}}. \quad (\text{A5})$$

The decreased \$\omega_{LPF}\$ gives rise to smoother changes of \$V_{dc}\$, thus enhancing the power quality of DC subgrid.

C. Phase Locked Loop (PLL) Control Diagram

In the proposed DPMS, conventional PLL is utilized to sense the frequency of AC subgrid. The control diagram of PLL is given in Fig. A4 where \$K_{pll}(s)\$ is a PI controller with the proportional gain and integral gain selected as 15 and 300 respectively.

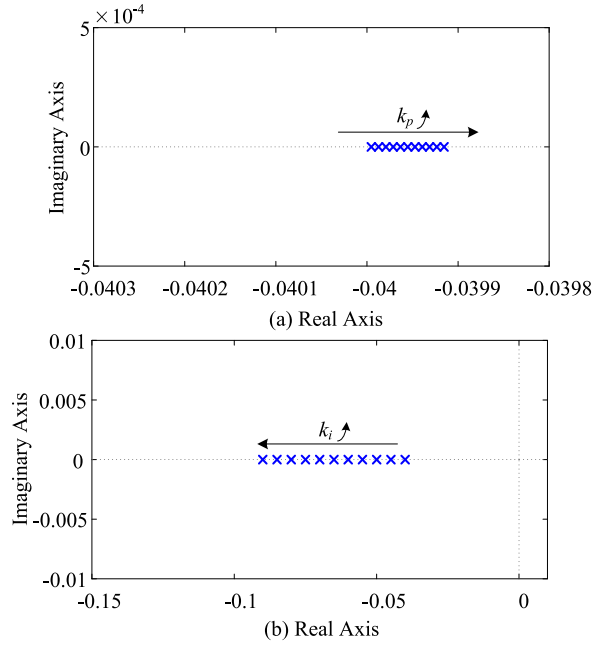


Fig. A5. Dominant eigenvalue loci of \$A_{sys}\$ with PI parameter variations in LDC. (a) \$k_p\$ increases from 2 to 22 with step of 2. (b) \$k_i\$ increases from 400 to 900 with step of 50.

D. Large Signal Dynamic Analyses of DPMS

The design of PI in LDC should be conducted before a particular BIC is put into service. In a practical operating system, the communication time delay would be unknown since it may change along with different circumstances, such as the aging of communication links. In this context, a better choice is to design proper \$k_p\$ and \$k_i\$ of LDC for the hybrid MG in an ideal case (without time delay), and anticipate that the PI parameters could tolerate a comparatively long communication time delay. On the other hand, to have a better view of how \$k_p\$ and \$k_i\$ can be chosen to enhance stability, the linearized small signal model, which is only valid around small vicinities of existing equilibriums, would not be suitable. Instead, large signal dynamic analyses should be performed to investigate the existences of equilibriums and the convergence speed of system parameters to the designated points.

Referring to (25), the error dynamic can be written below,

$$\dot{\mathbf{e}} = \alpha \mathbf{L} \mathbf{P}_{\max}^{-1} \mathbf{P}_{\text{ref}} + \mathbf{G} \boldsymbol{\beta} \mathbf{1}_x \mathbf{e}_{LC}. \quad (\text{A6})$$

where \$\mathbf{e} = [e_1 \dots e_k \dots e_x]^T\$. The hybrid MG system has equilibriums as long as the error vector \$\mathbf{e}\$ could be regulated to zero. Taking the derivative of (A6) yields

$$\begin{aligned} \dot{\mathbf{e}} &= \alpha \mathbf{L} \mathbf{P}_{\max}^{-1} \dot{\mathbf{P}}_{\text{ref}} + \mathbf{G} \boldsymbol{\beta} \mathbf{1}_x \dot{\mathbf{e}}_{LC} \\ \dot{\mathbf{P}}_{\text{ref}} &= k_p \mathbf{e} + k_i \int \mathbf{e} dt \Rightarrow \dot{\mathbf{P}}_{\text{ref}} = k_p \dot{\mathbf{e}} + k_i \mathbf{e}. \end{aligned} \quad (\text{A7})$$

For simplicity, it is assumed that \$k_p = k_{1p} = \dots k_{kp} = \dots k_{xp}\$ and \$k_i = k_{1i} = \dots k_{ki} = \dots k_{xi}\$. In (A7), substituting the second equation into the first one gives rise to

$$\begin{aligned} \dot{\mathbf{e}} &= \alpha \mathbf{L} \mathbf{P}_{\max}^{-1} (k_p \dot{\mathbf{e}} + k_i \mathbf{e}) + \mathbf{G} \boldsymbol{\beta} \mathbf{1}_x \Phi, \quad \dot{\mathbf{e}}_{LC} = \Phi \Rightarrow \\ \dot{\mathbf{e}} &= (\mathbf{I} - \alpha \mathbf{L} \mathbf{P}_{\max}^{-1} k_p)^{-1} \alpha \mathbf{L} \mathbf{P}_{\max}^{-1} k_i \mathbf{e} \\ &\quad + (\mathbf{I} - \alpha \mathbf{L} \mathbf{P}_{\max}^{-1} k_p)^{-1} \mathbf{G} \boldsymbol{\beta} \mathbf{1}_x \Phi. \end{aligned} \quad (\text{A8})$$

The dynamic of e incorporates an auxiliary state Φ which is exactly the first order differentiation of e_{LC} , and e_{LC} dynamic can be derived as

$$\begin{aligned}\dot{e}_{LC} &= \frac{\dot{V}_{dc}}{\Delta v} - \frac{\dot{f}_{ac}}{\Delta f} \Rightarrow \\ \dot{e}_{LC} &= -\omega_{LPF} e_{LC} - \omega_{LPF} \left(\frac{dP_{dc}}{\Delta v} - \frac{aP_{ac}}{\Delta f} \right) \\ &\quad - \omega_{LPF} \left(\frac{d}{\Delta v} + \frac{a}{\Delta f} \right) \mathbf{1}_x^T \mathbf{P}_{ref}. \end{aligned}\quad (\text{A9})$$

Taking the derivative of Φ results in

$$\begin{aligned}\dot{\Phi} &= \ddot{e}_{LC} = -\omega_{LPF} \dot{e}_{LC} - \omega_{LPF} \left(\frac{d}{\Delta v} + \frac{a}{\Delta f} \right) \mathbf{1}_x^T \dot{\mathbf{P}}_{ref} \Rightarrow \\ \dot{\Phi} &= -\omega_{LPF} \Phi - \omega_{LPF} \left(\frac{d}{\Delta v} + \frac{a}{\Delta f} \right) \mathbf{1}_x^T (\mathbf{k}_p \dot{e} + \mathbf{k}_i e). \end{aligned}\quad (\text{A10})$$

Substituting (A8) into (A10) and performing manipulations, an autonomous error model representing the overall MG in the large signal sense can be obtained,

$$\begin{bmatrix} \dot{e} \\ \dot{\Phi} \end{bmatrix} = \underbrace{\begin{bmatrix} \mathbf{a} & \mathbf{b} \\ \mathbf{c} & d \end{bmatrix}}_{A_{sys}} \begin{bmatrix} e \\ \Phi \end{bmatrix}. \quad (\text{A11})$$

where A_{sys} is system matrix. \mathbf{a} , \mathbf{b} , \mathbf{c} and d could be detailed as

$$\begin{aligned}\mathbf{a} &= \left(\mathbf{I} - \alpha \mathbf{L} \mathbf{P}_{max}^{-1} \mathbf{k}_p \right)^{-1} \alpha \mathbf{L} \mathbf{P}_{max}^{-1} \mathbf{k}_i, \mathbf{a} \in R^{x \times x} \\ \mathbf{b} &= \left(\mathbf{I} - \alpha \mathbf{L} \mathbf{P}_{max}^{-1} \mathbf{k}_p \right)^{-1} G \beta \mathbf{1}_x, \mathbf{b} \in R^{x \times 1} \\ \mathbf{c} &= -\omega_{LPF} \left(\frac{d}{\Delta v} + \frac{a}{\Delta f} \right) \mathbf{1}_x^T \left[\mathbf{k}_p \left(\mathbf{I} - \alpha \mathbf{L} \mathbf{P}_{max}^{-1} \mathbf{k}_p \right)^{-1} \alpha \mathbf{L} \mathbf{P}_{max}^{-1} \mathbf{k}_i + \mathbf{k}_i \right], \\ \mathbf{c} &\in R^{1 \times x} \\ d &= -\omega_{LPF} \left[1 + \left(\frac{d}{\Delta v} + \frac{a}{\Delta f} \right) \mathbf{1}_x^T \mathbf{k}_p \left(\mathbf{I} - \alpha \mathbf{L} \mathbf{P}_{max}^{-1} \mathbf{k}_p \right)^{-1} G \beta \mathbf{1}_x \right] \\ &\times d \in R^{1 \times 1} \end{aligned}$$

As long as A_{sys} in (A11) has all eigenvalues with negative real parts, the system is stable and the steady state operation point does exist. (A11) is a generalized large signal model which adapts to the MG with BICs connected in arbitrary communication graph. Concentrating on a specific hybrid MG as in Fig. 7 where three BICs are included and BIC₁ is the leader, with the corresponding parameters tabularized in TABLE I, the dominant eigenvalue loci of A_{sys} against LDC k_p and k_i variations are shown Fig. A5.

It is apparent from Fig. A5 that the increased k_p would drive the dominant pole moving toward imaginary axis, which narrows down the stability margin. In contrast, when k_i increases from 400 to 900 with step of 50, the dominant pole moves along with the negative horizontal axis. From the holistic perspective, smaller k_p and larger k_i would help to improve the system stability. With dominant pole having negative real part, the equilibrium of the hybrid MG exists, i.e.,

$$\lim_{t \rightarrow \infty} \mathbf{e} = \mathbf{0}, \lim_{t \rightarrow \infty} \Phi = 0. \quad (\text{A12})$$

The smaller real part of the dominant pole leads to the faster convergence speeds of e and Φ from their initial values to zero. However, $\Phi = 0$ does not necessarily imply that e_{LC} could be

0 in steady state. For this reason, solving (A11) in Laplace domain, $\mathbf{e}(s)$ and $\Phi(s)$ can be derived as

$$\begin{bmatrix} \mathbf{e}(s) \\ \Phi(s) \end{bmatrix} = [s\mathbf{I}_{(x+1) \times (x+1)} - A_{sys}]^{-1} \begin{bmatrix} \mathbf{e}_0 \\ \Phi_0 \end{bmatrix}. \quad (\text{A13})$$

where \mathbf{e}_0 and Φ_0 are the initial values. In accordance with modern control theory, the inversion of $s\mathbf{I} - A_{sys}$ can be calculated as,

$$\begin{aligned}[s\mathbf{I}_{(x+1) \times (x+1)} - \mathbf{B}]^{-1} &= \begin{bmatrix} s\mathbf{I}_{x \times x} - \mathbf{a} & -\mathbf{b} \\ -\mathbf{c} & s - d \end{bmatrix}^{-1} \\ &= \begin{bmatrix} (s\mathbf{I}_{x \times x} - \mathbf{a})^{-1} + (s\mathbf{I}_{x \times x} - \mathbf{a})^{-1} \mathbf{b} \Delta^{-1} \mathbf{c} (s\mathbf{I}_{x \times x} - \mathbf{a})^{-1} & (s\mathbf{I}_{x \times x} - \mathbf{a})^{-1} \mathbf{b} \Delta^{-1} \\ \Delta^{-1} \mathbf{c} (s\mathbf{I}_{x \times x} - \mathbf{a})^{-1} & \Delta^{-1} \end{bmatrix}. \end{aligned}\quad (\text{A14})$$

where $\Delta = (s - d) + \mathbf{c} (s\mathbf{I}_{x \times x} - \mathbf{a})^{-1} \mathbf{b}$.

Based on (A14), $\Phi(s)$ can be further computed as

$$\Phi(s) = \Delta^{-1} \mathbf{c} (s\mathbf{I}_{x \times x} - \mathbf{a})^{-1} \mathbf{e}_0 + \Delta^{-1} \Phi_0. \quad (\text{A15})$$

Considering the MG in Fig. 7 again and substituting relevant parameters in TABLE I into (A15), it is true that $\mathbf{e}_0 = [e_{LC0}, 0, 0]^T$ and $\Phi_0 = 0$. Then $\Phi(s)$ could be concretized as

$$\Phi(s) = \frac{-200\beta_1 e_{LC0}}{10s^2 + 5001s + 400}. \quad (\text{A16})$$

Note that the Laplace domain expression of e_{LC} dynamic can be delineated by

$$e_{LC}(s) = \frac{1}{s} [e_{LC0} + \Phi(s)] = \frac{1}{s} \left[e_{LC0} - \frac{200\beta_1 e_{LC0}}{10s^2 + 5001s + 400} \right]. \quad (\text{A17})$$

As recorded in TABLE I, β_1 equals 2. Evaluating final value theorem on (A17) gives the steady state value of e_{LC} in the time domain, i.e.,

$$\lim_{t \rightarrow \infty} e_{LC} = \lim_{s \rightarrow 0} s e_{LC}(s) = \lim_{s \rightarrow 0} \left[e_{LC0} - \frac{200 \cdot 2 \cdot e_{LC0}}{10s^2 + 5001s + 400} \right] = 0. \quad (\text{A18})$$

Through above theoretical analyses, it can be summarized that by using the proposed LDC, the difference (e_{LC}) of AC and DC LCs can be enforced to zero in steady state. The smaller k_p and larger k_i in LDCs will drive the dominant pole moving into more stable region, thus ensuring the existences of equilibriums and speeding up the convergence rate of error dynamics.

REFERENCES

- [1] S. Morozumi, H. Nakama, and N. Inoue, "Demonstration projects for grid-connection issues in Japan," *Elektrotechnik Und Informationstechnik*, vol. 125, no. 12, pp. 426–431, Dec. 2008.
- [2] F. Nejabatkhah and Y. W. Li, "Overview of power management strategies of hybrid AC/DC microgrid," *IEEE Trans. Power Electron.*, vol. 30, no. 12, pp. 7072–7089, Dec. 2015.
- [3] I. Mitra, T. Degner, and M. Braun, "Distributed generation and microgrids for small island electrification in developing countries? A review," *Sol. Energy Soc. India*, vol. 18, no. 1, pp. 6–20, 2008.
- [4] D. Van Hertem, M. Ghandhari, and M. Delimar, "Technical limitations towards a supergrid—A European prospective," in *Proc. IEEE Int. Energy Conf.*, 2010, pp. 302–309.
- [5] L. Asiminoaei, E. Aeloiza, P. N. Enjeti, and F. Blaabjerg, "Shunt active-power-filter topology based on parallel interleaved inverters," *IEEE Trans. Ind. Electron.*, vol. 55, no. 3, pp. 1175–1189, Mar. 2008.

- [6] Z. Ye, D. Boroyevich, J. Y. Choi, and F. C. Lee, "Control of circulating current in two parallel three-phase boost rectifiers," *IEEE Trans. Power Electron.*, vol. 17, no. 5, pp. 609–615, Sep. 2002.
- [7] D. Sha, Z. Guo, and X. Liao, "Control strategy for input-parallel-output-parallel connected high-frequency isolated inverter modules," *IEEE Trans. Power Electron.*, vol. 26, no. 8, pp. 2237–2248, Aug. 2011.
- [8] R. Zhu, M. Liserre, Z. Chen, and X. Wu, "Zero-sequence voltage modulation strategy for multiparallel converters circulating current suppression," *IEEE Trans. Ind. Electron.*, vol. 64, no. 3, pp. 1841–1852, Mar. 2017.
- [9] Y. H. Liao and H. C. Chen, "Simplified PWM with switching constraint method to prevent circulating currents for paralleled bidirectional AC/DC converters in grid-tied system using graphic analysis," *IEEE Trans. Ind. Electron.*, vol. 62, no. 7, pp. 4573–4586, Jul. 2015.
- [10] J. Xiao, P. Wang, and L. Setyawan, "Implementation of multiple-slack-terminal DC microgrids for smooth transitions between grid-tied and islanded states," *IEEE Trans. Smart Grid*, vol. 7, no. 1, pp. 273–281, Jan. 2016.
- [11] P. C. Loh, D. Li, Y. K. Chai, and F. Blaabjerg, "Autonomous operation of hybrid microgrid with AC and DC subgrids," *IEEE Trans. Power Electron.*, vol. 28, no. 5, pp. 2214–2223, May 2013.
- [12] S. K. Mazumder, M. Tahir, and K. Acharya, "Master-slave current-sharing control of a parallel DC–DC converter system over an RF communication interface," *IEEE Trans. Ind. Electron.*, vol. 55, no. 1, pp. 59–66, Jan. 2008.
- [13] T.-F. Wu, Y.-K. Chen, and Y.-H. Huang, "3C strategy for inverters in parallel operation achieving an equal current distribution," *IEEE Trans. Ind. Electron.*, vol. 47, no. 2, pp. 273–281, Apr. 2000.
- [14] C. Jin, J. Wang, K. L. Hai, C. F. Hoong, and P. Wang, "Coordination secondary control for autonomous hybrid AC/DC microgrids with global power sharing operation," in *Proc. IECON 42nd Annu. Conf. IEEE Ind. Electron. Soc.*, 2016, pp. 4066–4071.
- [15] X. Lu *et al.*, "Hierarchical control of parallel AC–DC converter interfaces for hybrid microgrids," *IEEE Trans. Smart Grid*, vol. 5, no. 2, pp. 683–692, Mar. 2014.
- [16] Y. Xia, Y. Peng, P. Yang, M. Yu, and W. Wei, "Distributed coordination control for multiple bidirectional power converters in a hybrid AC/DC microgrid," *IEEE Trans. Power Electron.*, vol. 32, no. 6, pp. 4949–4959, Jun. 2017.
- [17] Y. Xia, W. Wei, Y. Peng, P. Yang, and M. Yu, "Decentralized coordination control for parallel bidirectional power converters in a grid-connected DC microgrid," *IEEE Trans. Smart Grid*, vol. 9, no. 6, pp. 6850–6861, Nov. 2018.
- [18] V. Nasirian, A. Davoudi, F. L. Lewis, and J. M. Guerrero, "Distributed adaptive droop control for DC distribution systems," *IEEE Trans. Energy Convers.*, vol. 29, no. 4, pp. 944–956, Dec. 2014.
- [19] X. Li *et al.*, "A unified control for the DC–AC interlinking converters in hybrid AC/DC microgrids," *IEEE Trans. Smart Grid*, vol. 9, no. 6, pp. 6540–6553, Nov. 2018.
- [20] S. Peyghami, H. Mokhtari, and F. Blaabjerg, "Autonomous operation of a hybrid AC/DC microgrid with multiple interlinking converters," *IEEE Trans. Smart Grid*, vol. 9, no. 6, pp. 6480–6488, Nov. 2018.
- [21] P. Yang, Y. Xia, M. Yu, W. Wei, and Y. Peng, "A decentralized coordination control method for parallel bidirectional power converters in a hybrid AC–DC microgrid," *IEEE Trans. Ind. Electron.*, vol. 65, no. 8, pp. 6217–6228, Aug. 2018.
- [22] J. He and Y. W. Li, "Analysis, design, and implementation of virtual impedance for power electronics interfaced distributed generation," *IEEE Trans. Ind. Appl.*, vol. 47, no. 6, pp. 2525–2538, Nov. 2011.
- [23] H. Han, Y. Liu, Y. Sun, M. Su, and J. M. Guerrero, "An improved droop control strategy for reactive power sharing in islanded microgrid," *IEEE Trans. Power Electron.*, vol. 30, no. 6, pp. 3133–3141, Jun. 2015.
- [24] J. M. Guerrero, L. G. de Vicuna, J. Matas, J. Miret, and M. Castilla, "Output impedance design of parallel-connected UPS inverters," in *Proc. IEEE Int. Symp. Ind. Electron.*, vol. 2, 2004, pp. 1123–1128.
- [25] P. Wang *et al.*, "Distributed control for autonomous operation of a three-port AC/DC/DS hybrid microgrid," *IEEE Trans. Ind. Electron.*, vol. 62, no. 2, pp. 1279–1290, Feb. 2015.
- [26] G. Fanghong, W. Changyun, and Y.-D. Song, *Distributed Control and Optimization Technologies in Smart Grid Systems*. Boca Raton, FL, USA: CRC Press, 2017.
- [27] F. Guo, Q. Xu, C. Wen, L. Wang, and P. Wang, "Distributed secondary control for power allocation and voltage restoration in islanded DC microgrids," *IEEE Trans. Sustain. Energy*, vol. 9, no. 4, pp. 1857–1869, Oct. 2018.
- [28] F. Guo, C. Wen, J. Mao, and Y.-D. Song, "Distributed secondary voltage and frequency restoration control of droop-controlled inverter-based microgrids," *IEEE Trans. Ind. Electron.*, vol. 62, no. 7, pp. 4355–4364, Jul. 2015.
- [29] A. Bidram, F. L. Lewis, and A. Davoudi, "Distributed control systems for small-scale power networks: Using multiagent cooperative control theory," *IEEE Control Syst. Mag.*, vol. 34, no. 6, pp. 56–77, Dec. 2014.
- [30] X. Lu, J. M. Guerrero, K. Sun, and J. C. Vasquez, "An improved droop control method for DC microgrids based on low bandwidth communication with DC bus voltage restoration and enhanced current sharing accuracy," *IEEE Trans. Power Electron.*, vol. 29, no. 4, pp. 1800–1812, Apr. 2014.
- [31] X. Li *et al.*, "Wide damping region for LCL-type grid-connected inverter with an improved capacitor-current-feedback method," *IEEE Trans. Power Electron.*, vol. 30, no. 9, pp. 5247–5259, Sep. 2015.
- [32] Y. Tang, W. Yao, P. C. Loh, and F. Blaabjerg, "Design of LCL filters with LCL resonance frequencies beyond the Nyquist frequency for grid-connected converters," *IEEE J. Emerg. Sel. Top. Power Electron.*, vol. 4, no. 1, pp. 3–14, Mar. 2016.
- [33] S. Bacha, I. Munteanu, and A. I. Brateu, *Power Electronic Converters Modeling and Control*, vol. 454. London, U.K.: Springer, 2014.
- [34] P. C. Loh, D. Li, Y. K. Chai, and F. Blaabjerg, "Hybrid AC–DC microgrids with energy storages and progressive energy flow tuning," *IEEE Trans. Power Electron.*, vol. 28, no. 4, pp. 1533–1543, Apr. 2013.
- [35] E. Rodriguez-Diaz *et al.*, "Voltage-level selection of future two-level LVdc distribution grids: A compromise between grid compatibility, safety, and efficiency," *IEEE Electrific. Mag.*, vol. 4, no. 2, pp. 20–28, Jun. 2016.
- [36] X. Li *et al.*, "Observer-based DC voltage droop and current feed-forward control of a DC microgrid," *IEEE Trans. Smart Grid*, vol. 9, no. 5, pp. 5207–5216, Sep. 2018.
- [37] Z. Li and M. Shahidehpour, "Small-signal modeling and stability analysis of hybrid AC/DC microgrids," *IEEE Trans. Smart Grid*, vol. 10, no. 2, pp. 2080–2095, 2019.
- [38] J. Fang, X. Li, H. Li, and Y. Tang, "Stability improvement for three-phase grid-connected converters through impedance reshaping in quadrature-axis," *IEEE Trans. Power Electron.*, vol. 33, no. 10, pp. 8365–8375, Oct. 2018.
- [39] F. M. Hughes, "Power system control and stability," *Electron. Power*, vol. 23, no. 9, p. 739, 1977.



Pengfeng Lin (S'16) received the B.S. and M.S. degrees in electrical engineering from Southwest Jiaotong University, China, in 2013 and 2015, respectively. He is currently pursuing the Ph.D. degree with the Interdisciplinary Graduate School, ERI@N, Nanyang Technological University, Singapore. His research interests include energy storage systems, hybrid ac/dc microgrids, and electrical power system stability analyses.



Peng Wang (M'00–SM'11–F'18) received the B.Sc. degree in electrical engineering from Xian Jiaotong University, China, in 1978, the M.Sc. degree in electrical engineering from the Taiyuan University of Technology, China, in 1987, the M.Sc. and Ph.D. degrees in electrical engineering from the University of Saskatchewan, Canada, in 1995 and 1998, respectively. He is currently a Professor with Nanyang Technological University, Singapore.



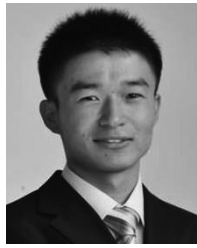
Chi Jin received the B.Sc. degree in electrical engineering from Wuhan University, Wuhan, China, in 2007 and the M.Sc. and Ph.D. degrees from the School of Electrical and Electronic Engineering, Nanyang Technological University, Singapore, in 2008 and 2013, respectively.

In 2011, he was a Visiting Scholar with the Institute of Energy Technology, Aalborg University, Aalborg, Denmark, where he worked on the control strategies of hybrid ac/dc/storage microgrid system. Since 2013, he has been with the Energy Research

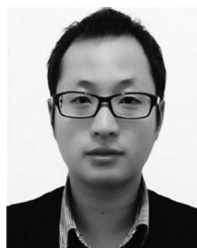
Institute @ Nanyang Technological University, Singapore, as a Research Fellow.



Fanghong Guo (S'15–M'16) received the B.Eng. degree in automation science from Southeast University, Nanjing, China, in 2010, the M.Eng. degree in automation science and electrical engineering from Beihang University, Beijing, China, in 2013, and the Ph.D. degree in sustainable earth from the Interdisciplinary Graduate School, Energy Research Institute @ NTU, Nanyang Technological University, Singapore, in 2016. He is currently with the Department of Automation, Zhejiang University of Technology, Hangzhou, China. His research interests include distributed cooperative control, distributed optimization on microgrid systems, and smart grid.



Jianfang Xiao (S'11–M'16) received the B.Sc. degree (Hons.) in mechanical engineering from the School of Mechanical and Aerospace Engineering, Nanyang Technological University (NTU) in 2011 and the Ph.D. degree in electrical engineering from the School of Electrical and Electronic Engineering, NTU, in 2015. He is current an Assistant Professor with Newcastle University in Singapore.



Xiaoqiang Li (M'16) received the B.S. degree in electrical engineering and automation and the Ph.D. degree in electrical engineering from the School of Information and Electrical Engineering, China University of Mining and Technology, Xuzhou, China, in 2010 and 2015, respectively. From 2015 to 2018, he was a Research Fellow with Nanyang Technological University, Singapore. Since 2018, he has been an Associate Professor with the China University of Mining and Technology. His research interests include renewable energy generation and digital control in power electronics.



Chuanlin Zhang (M'14) received the B.S. degree in mathematics and the Ph.D. degree in control theory and control engineering from the School of Automation, Southeast University, Nanjing, China, in 2008 and 2014, respectively. He was a visiting Ph.D. student with the Department of Electrical and Computer Engineering, University of Texas at San Antonio, USA, from 2011 to 2012, and a Visiting Scholar with the Energy Research Institute @ NTU, Nanyang Technological University, Singapore, from 2016 to 2017 and the Advanced Robotics Center, National University of Singapore from 2017 to 2018. Since 2014, he has been with the College of Automation Engineering, Shanghai University of Electric Power, Shanghai, where he is currently a full Professor.

He is the Principal Investigator of several research projects, including Leading Talent Program of Shanghai Science and Technology Commission and Chengguang Program by the Shanghai Municipal Education Commission. His research interests include nonlinear system control theory and applications for power systems. He was a recipient of the Best Poster Paper Award from the 3rd International Federation of Automatic Control International Conference on Intelligent Control and Automation Science in 2013. He serves as a Guest Editor for *Energies*.